Investigation on RELAP5-3D© capability to predict thermal stratification in liquid metal pool-type system and comparison with experimental data

Vincenzo Narcisi, Fabio Giannetti, Gianfranco Caruso

DIAEE – Nuclear Section, “Sapienza” University of Rome, Corso Vittorio Emanuele II, 244, 00186, Rome, Italy

Narcisi V., Giannetti F., Caruso G., 2019. Investigation on RELAP5-3D© capability to predict thermal stratification in liquid metal pool-type system and comparison with experimental data. Nucl. Eng. and Des., 352 (110152)
https://doi.org/10.1016/j.nucengdes.2019.110152

ABSTRACT

A numerical activity, aimed to evaluate the capability of RELAP5-3D© to reproduce the main thermal-hydraulic phenomena in an HLM pool-type facility, in different operative conditions, is presented. For this purpose, the experimental campaign performed in CIRCE-ICE test facility has been selected for the code assessment. Two experimental tests have been analyzed: TEST A consisting in a transition from no-power to a full power steady state conditions, and TEST I, consisting in a transition from gas-enhanced circulation to natural circulation, simulating a protected loss of heat sink plus a loss of flow accident. Three different pool modelling approaches are presented, consisting in a single vertical pipe, parallel pipes with cross junctions and multi-dimensional component. The comparison with experimental data has highlighted the need to divide the large pool in several sections to reproduce the natural convection, strictly correlated with the thermal stratification. The multi-dimensional component seems to be the best practice for the evaluation of this phenomenon even if the lack of specific correlation for heat transfer coefficient in quasi-stagnant conditions in large tanks is a limit for the accuracy of the results. In addition, the paper presents a detailed nodalization of the fuel pin bundle, highlighting quite good capabilities of RELAP5-3D as a subchannel analysis code.

Keywords

- CIRCE-ICE facility; Gas-enhanced circulation; Natural Circulation; Code Validation; Safety analysis; Transient simulation

1. Introduction

The Lead-cooled Fast Reactor (LFR) belongs to the concepts individuated by Generation IV International Forum (GIF) for Generation IV (Gen IV) (OECD Nuclear Energy Agency, 2017). The LFR system is characterized by a fast neutron spectrum and it includes both lead and lead bismuth eutectic alloy (LBE) as coolant. These two liquid metals offer several advantages in terms of interaction with structural materials, neutron economic and thermal-hydraulic behavior.

In the framework of LEADER project (Lead-cooled European Advanced DEmonstration Reactor) the development of an LFR scaled demonstrator was proposed, called ALFRED (Advanced Lead Fast Reactor European Demonstrator). ALFRED was conceived as a lead-cooled pool type reactor, where the whole primary system, including the primary pumps and the steam generators, was submerged in a large lead pool inside the primary vessel walls (Frogheri et al., 2013). This concept allows the elimination of all problems related to the out-of vessel primary system, but some critical points are introduced.

One of the most relevant safety aspects related to a quasi-stagnant heavy liquid metal (HLM) pool is the thermal stratification phenomenon. This expression identifies the separation between the hot and the cold liquid layers inside the pool. The phenomenon has been already studied in the past, related to the light water-cooled reactors, where the thermal stratification can occur in the piping system (Kadambi, 1988; Thuy et al., 2012; Schuler et al., 2004) or inside the pressurizer, or to the thermal-hydraulics of passive safety systems where large tank at low pressure operates as heat sink (D'Auria, 2017).

In HLM pool-type systems the thermal stratification is due to the heat losses from the internal component and towards the external environment. The hot fluid, heated by the internals, moves upward staying in the upper volume of the pool, while the cold liquid metal is confined, forming layers at different temperature inside the pool. The thermal stratification is an important aspect for the safety of the nuclear power plants as it affects the structural integrity of the reactor, causing fatigue in nuclear components.

Different modelling approaches are available in literature for the evaluation of the thermal stratification in large pools. They are related to the numerical tools adopted: thermal-hydraulic system (TH-SYS) or Computational Fluid Dynamics (CFD) codes.

RELAP5, specifically the RELAP5-3D code, has been developed at Idaho National Laboratory (INL) for the thermal-hydraulic analyses of nuclear systems. RELAP5 uses a

first-order semi-implicit upwind differencing scheme which leads to an axial artificial mixing of the hot and cold fluids that does not allow an accurate evaluation of a sharp thermal front. For this reason, a thermal stratification model was implemented in RELAP5. This model is based on HARTEN's subcell resolution scheme (Harten, 1989), tracking the thermal front in the interior of the control volume instead at the edge of the cell as in system codes (The RELAP5-3D© Code Development Team, 2015a). This approach allows a good evaluation of the thermal stratification when a relatively coarse nodalization is applicable, such as the pressurizer modelling case. Based on the experimental campaign carried out by Saedi (1983) and Kim (1984), simulation activities performed by Shumway et al. (2002) and Bayless et al. (2015) assessed the capability of RELAP5 to reproduce thermal stratification phenomenon in the pressurizer, modelling the component with a single vertical pipe and adopting the stratification model. The computational activity has been repeated by Ahn et al. (2018) investigating the influence of the number of nodes on the evaluation of the thermal stratification. The simulations highlighted good agreement with the experiment when the nodalization scheme is sufficiently fine, 10 nodes in this case. When the number of nodes is increased to 20, the calculation observed negligible improvement in the results.

When the multi-dimensional effects are relevant, such as in large tanks, the modelling approach described above shows limitations on the evaluation of the stratification. This is the results highlighted by Verma et al. (2013) comparing the simulations (using RELAP5/MOD3.2) with the experimental campaign conducted on an isolation condenser immersed in a gravity driven water tank. A different approach was applied by Kumar et al. (2017), modelling the large tank with three parallel pipes and cross junctions to simulate the buoyancy inside the pool. Due to the cross junctions, the thermal stratification model could not be activated, so a detailed nodalization (more than 50 volumes per each pipe) of the tank was necessary to predict the thermal front. This modification led to a better estimation of the experimental results. A similar approach was used by Hou et al. (2017) using RELAP5/MOD3.3 to reproduce a passive containment cooling system (PCCS) with open natural circulation. The pool was reproduced with four parallel pipes (20 control volumes per each pipe) with cross junction highlighting the goodness of this modelling approach on the evaluation of the thermal stratification in large volumes.

The modelling guidelines obtained for the simulation of large volume in LWR system, were used by Bandini et al. (2015) to assess the capability of RELAP5/MOD3.3, modified with the implementation of lead alloy thermophysical properties by ENEA and Ansaldo, to reproduce

the thermal-hydraulics of an LBE-cooled pool-type facility, called CIRCE. The modelling approach was to divide the upper part of the pool, where relevant stratification was expected to occur, in three parallel vertical pipes with cross junction; the lower part was modelled with a single vertical channel. The results showed a good qualitative temperature trend inside the pool, even if some discrepancies were observed in the middle of the pool. The same experimental campaign was analyzed by “Sapienza” University of Rome using RELAP5-3D. In this version of the code, a multi-dimensional modeling capability was introduced to allow the user to model more accurately reactor components where three-dimensional effects are expected to be relevant, such as core, core bypass or downcomer. In Narcisi et al. (2017), the multi-dimensional component was used to model the LBE pool of CIRCE facility. The analysis highlighted good capabilities of the three-dimensional component to reproduce thermal stratification in an HLM pool, providing a good estimation of the temperature in the upper and lower zone of the pool. However, the relevant stratification at the middle of the pool was not observed by the simulations.

A different approach of the pool modelling is to use CFD codes. Being these analyses expensive in terms of computational cost, two approaches were proposed in literature: to reproduce the pool only with CFD codes, imposing boundary conditions obtained from TH-SYS calculation, or to perform a TH-SYS/CFD coupled calculation. The first approach was used by “Sapienza” University of Rome (Edemetti et al., 2018). CIRCE pool was modelled using ANSYS-CFX v15.0 and the primary system of the facility was assumed as boundary conditions, in terms of heat losses calculated by RELAP5-3D calculations (Narcisi et al., 2017). The simulation activity showed improved results on the evaluation of the vertical temperature trend, highlighting a better capability on the reproduction of 3D flow of the LBE in comparison with the TH-SYS calculations. The second approach was used by University of Pisa that developed a coupling methodology, combining the best features of TH-SYS and CFD codes (Angelucci et al., 2017).

Starting from the actual state of art in the pool modelling, in this study the capability of RELAP5-3D to predict thermal stratification inside a large LBE pool is assessed. For this purpose, the experimental campaign carried out on CIRCE facility provided useful experimental data. The nodalization scheme presented in Narcisi et al (2017) has been improved to better reproduce the heat losses towards the pool and the external environment.

2. Experimental campaign

2.1 CIRCE-ICE facility description

CIRCE (CIRColazione Eutettico) is a multifunctional pool-type facility aimed to investigate innovative HLM systems. The facility consists of three tanks: the main vessel and two auxiliary tanks. The main vessel, filled with about 70 tons of molten LBE, has been designed to host different test sections, welded to and hung from the bolted heads. It is characterized by the outer diameter of 1200 mm and the height of 8500 mm and the whole surface is thermally insulated, except for the cover head. The auxiliary tanks are needed to store LBE during the maintenance phases and to provide an expansion volume during the loading and the drainage phases (Turroni et al., 2001).

Fig. 1 depicts the test section, called ICE (Integral Circulation Experiment), implemented in the CIRCE pool to simulate the primary system of an HLM-cooled pool-type reactor. The main components can be identified in Fig. 1 where the primary main flow path is shown. The cold LBE enters the test section through the feeding conduit, at the bottom of the facility. The feeding conduit is equipped with a Venturi-nozzle flow meter to measure the LBE mass flow rate entering the heat source (HS). Crossing a lower grid, the LBE moves inside the fuel pin simulator (FPS), where it is heated by 37 electrically heated pins. The FPS is divided into three axial regions, individuated by three spacer grids the first one positioned between the bottom mixing zone and the active length inlet (in red in Fig. 1), the second one at the middle of the HS and the third region between the active length outlet and the upper mixing zone. The heat source consists of an electrical pin bundle characterized by a nominal thermal power of 800 kW and an active length of 1000 mm. The pins, characterized by the outer diameter of 8.2 mm, provide a thermal power of 25 kW and a heat flux at the pin wall of 1 MW/m^2. They are arranged in a wrapped hexagonal lattice with a pitch to diameter ratio (p/d) equal to 1.8 and they are kept in positions with the lower grid, three spacer grids and an upper grid, that operates as the FPS cap (Narcisi et al., 2018). The upper grid forces liquid metal to exit the FPS through six lateral holes, moving inside the fitting volume, a large component which collects the hot LBE and guarantees the connection between the HS and the riser. The riser is a double wall pipe insulated with the air gap in order to reduce the heat dissipation towards the pool. A nozzle is installed at the riser inlet to inject argon inside the molten metal, enhancing the circulation of the primary coolant. The argon pipe line descends through the LBE pool, passing through the facility cover head. The mixture Ar-LBE flows upward and it is collected inside the separator, which is the upper component of the test

section. The separator has two main purposes: to allow the separation of the mixture and to provide an expansion volume. Argon moves upward towards the gas plenum and the molten LBE enters the heat exchanger (HX). Fig. 2 shows the radial and azimuthal disposition of the primary main components. The riser outlet and the HX inlet are included inside the separator. The FPS is positioned below the dead volume allowing the passage of the power supply rods which feed the HS. The dead volume consists of two concentric pipes thermally insulated with a non-conductive material which partially fills the annular volume between the two pipes. Because of the power dissipated by Joule effect, a dedicated air-cooling system is adopted and included inside the inner pipe (Tarantino et al., 2011).

The heat exchanger is composed of 91 water-cooled bayonet tubes, arranged in a triangular bundle (p/d equal to 1.22) and characterized by an active length of 3462 mm. LBE flows downward through the free volume between the cylindrical shroud and the tubes, decreasing the temperature. Fig. 3 shows a schematic view of the bayonet tube, composed of three concentric tubes; the feed-water enters the unit at the inner tube top edge, it flows downward reaching the lower plenum of the bayonet element and then it flows upward inside through the annular riser. The volume between second and third tube is filled with pressurized helium to detect any leakage or rupture.

The decay heat removal (DHR) system is inside the pool, as shown in Fig. 1 and Fig. 2. The DHR is composed of one air-cooled bayonet tube included inside a double wall insulated shell with a thin air insulation gap to reduce the heat losses towards the pool. LBE enters the unit through six inlet holes obtained at the upper zone of the shell and then it flows downward.

The test facility is equipped with several thermocouples (TCs) to investigate the thermal behavior of the LBE. For this purpose, the FPS is supplied by 36 TCs arranged at seven axial levels. Two series of penetration are obtained at both inlet and outlet level of the HS active length to measure the temperature drop across three subchannels; in addition, four different sections are monitored: 60 mm downward the lower spacer grid, 20 mm upward the middle spacer grid, on the mid plane of the middle spacer grid and 60 mm upward the upper spacer grid. In each section, the temperature of three different subchannels is acquired. The temperature of the pin outer wall is also monitored in different axial levels (18 TCs). Flowing through the primary flow path, the LBE temperature is measured at inlet and outlet of the riser and the HX (Tarantino et al., 2015).

One of the main tasks of the experiment was to study mixing convection and thermal stratification inside the pool. For this purpose, 119 TCs are installed on 9 vertical rods arranged inside the pool (from A to I in Fig. 2) measuring the LBE temperature in 17 axial levels along the pool. The TCs axial positions are individuated in Fig. 1 for the B rod. As shown, the TCs disposition is intensified between the HX and DHR outlets, where a relevant thermal stratification was expected to occur. In addition, the LBE inlet and outlet temperature of the DHR is acquired with 12 TCs (Tarantino et al., 2015).

An evaluation of the thermocouple measurement uncertainties was performed by Martelli et al. (2015), where the global uncertainty is considered composed by the instrument uncertainty and the standard deviation of the temperature measurement. The same approach has been adopted in this analysis. In addition, the calibration and the accuracy estimation of the Venturi flow meter were analyzed in previous experimental campaign, described in Ambrosini et al. (2004) and Agostini et al. (2005). For an LBE mass flow rate around 50 kg/s, a relative error of about 25% was evaluated.

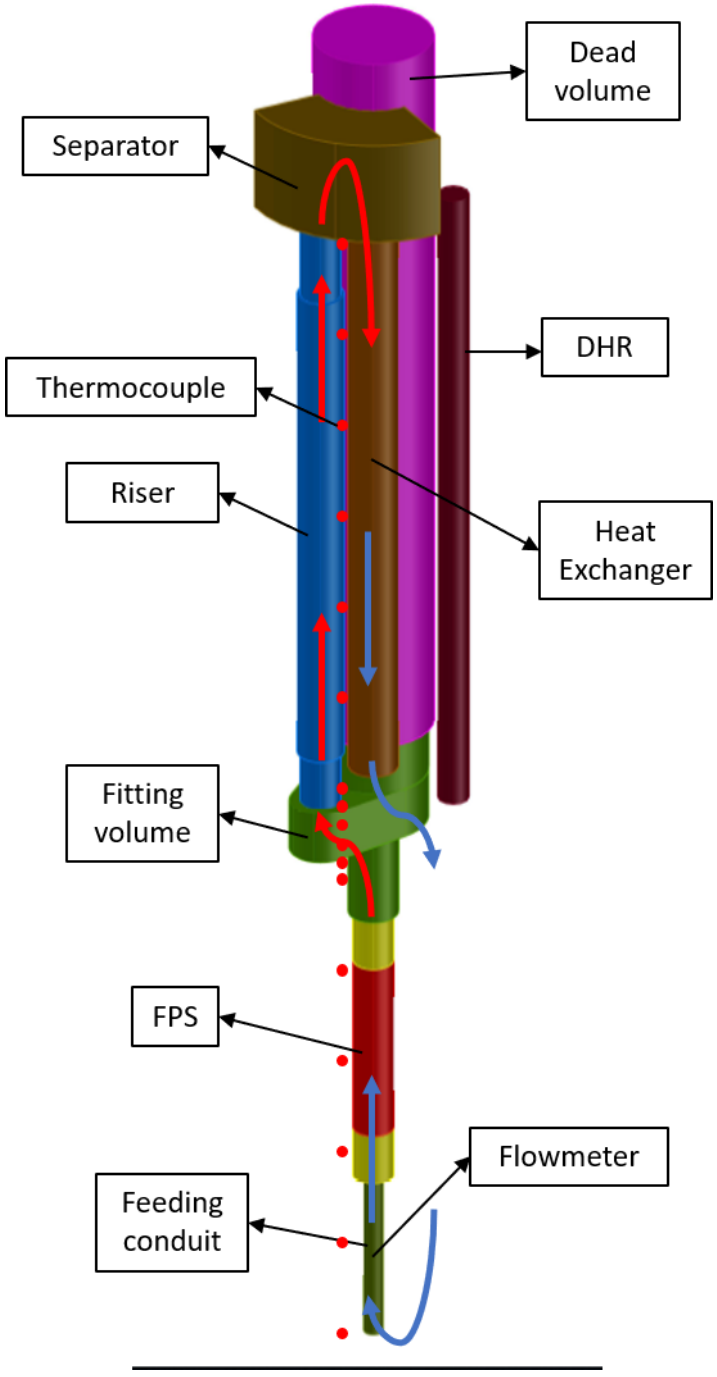

Fig. 1. CIRCE-ICE flow path

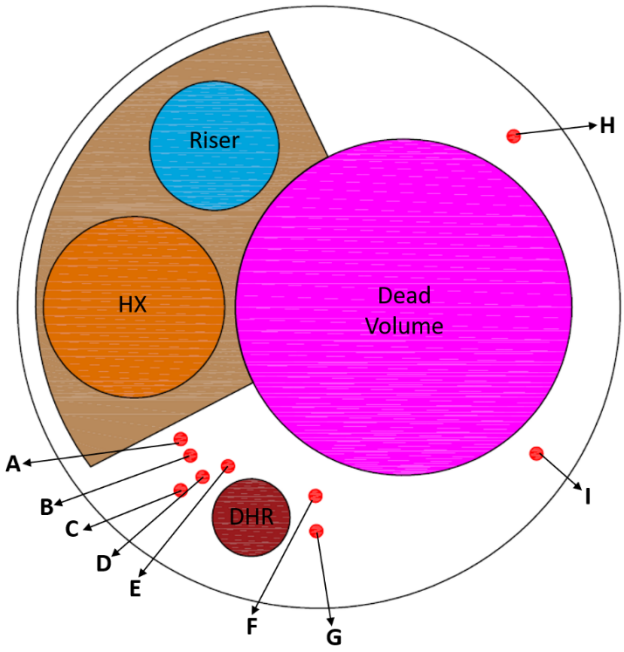

Fig. 2. ICE Test Section

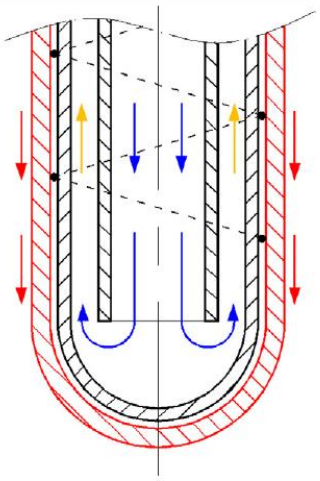

Fig. 3. HX bayonet tube (Bandini et al., 2015)

2.2 Experimental test

The objective of the experimental campaign was to investigate the main phenomena occurring in an HLM pool. Two tests have been considered in this paper: TEST A (Martelli et al., 2016) and TEST I (Tarantino et al., 2015).

TEST A starts in static conditions, where the FPS is turned-off and injection of Ar and feed-water is disabled. After about 600 s, the argon is injected inside the test section and, with a delay time of about 500 s, the FPS starts to supply thermal power reaching the nominal value of 800 kW in 180 s. After the achievement of the full power, feed-water (FW) starts to

flow on the HX secondary side with a mass flow rate of 0.6 kg/s. The boundary conditions are maintained constant for the duration of the test.

TEST I consists of a protected loss of heat sink (PLOHS) plus loss of flow (LOF) simulating the total loss of primary flow, the loss of secondary circuit, the consequent scram of the reactor and the activation of the DHR system. It aims to analyze the transition of thermal stratification inside the pool, passing from gas-enhanced circulation (GEC) to natural circulation (NC) conditions. The test starts in static conditions; after 450 s, argon is injected to obtain a “forced” circulation condition and the FPS is activated with a delay time of about 470 s. The full power of 730 kW is obtained at 1100 s and at this time the feed-water starts to circulate on the secondary side. These conditions are maintained for 25000 s, when the transition from GEC to NC occurs. The accident is reproduced reducing to zero the argon injection and the feed-water circulation. The HS thermal power decreases to 7% of the nominal value, following a typical decay heat curve for a HLM fast reactor and the DHR secondary side is fed by 0.223 kg/s of air.

The chronology of the two tests is summarized in Tab. 1.

Full power calculation		
Test	Event	Time (s)
A	Ar injection	600 → END
	FPS power ramp	1100 → 1280
	FPS full power	1280 → END
	FW injection	1280 → END
I	Ar injection	450 → 25400
	FPS power ramp	920 → 1100
	FPS full power	1100 → 25300
	FW injection	1100 → 25400
Transient calculation		
Test	Event	Time (s)
I	Ar injection disabled	25400 → END
	FW disabled	25400 → END
	FPS power ramp	25300 → 25430
	FPS decay heat value	25430 → END
	Air Injection	25440 → END

Tab. 1. Experimental tests: time events

3. Thermal-hydraulic model

RELAP5-3D© represents the latest version of the series RELAP5, a highly generic system code used not only for the best-estimate transient simulation of light water reactors, but also for simulations concerning a wide variety of thermal-hydraulic transients in non-nuclear systems. The main improvements included in RELAP5-3D© (R5-3D) are the fully integrated multi-dimensional thermal-hydraulic and kinetic modelling capabilities. The multi-dimensional (MULTID) component has been conceived to allow the model of multi-dimensional flow behavior that can occur in reactor applications, such as core, downcomer or steam generators. The enhancements of the latest version also include the addition of new working fluids, such as lead or LBE, for the simulation of Gen IV NPP (The RELAP5-3D© Code Development Team, 2015a).

The activity aims to investigate the capability of the code to reproduce the main thermal-hydraulic phenomena occurring in an HLM pool-type facility. To assess R5-3D ability, a mesh sensitivity analysis was carried out, including both main flow path and pool of the facility. The mesh influence on the calculations is presented in section 5. In this section, two basic nodalization approaches are presented and the main results are discussed in section 4.

The first geometrical scheme (model #1) consists of a mono-dimensional model of the whole facility. The nodalization is showed in Fig. 4. The model includes each component described in previous section and reported with different colors in Fig. 4. The feeding conduit (in green) is simulated using a pipe component, in which the Venturi flow meter is reproduced with a local pressure drop coefficient, dependent on the flow conditions (The RELAP5-3D© Code Development Team, 2015b) and validated in previous computational activity (Narcisi et al., 2017):

$$K_{Venturi} = 10.5\, Re^{-0.016}$$

where *Re* is the Reynolds number evaluated in the feeding conduit. The grids installed in the test section are also simulated with local pressure drops coefficients, evaluated with the Rehme correlation (Schikorr et al., 2010):

$$\Delta p_{grid} = C_v \cdot \varepsilon^2 \cdot 0.5 \cdot \rho \cdot v^2$$

where ρ and v are respectively fluid density and velocity and ε represents the grid flow blockage factor, calculated as:

$$\varepsilon = \frac{A_{grid}}{A_{flow}}$$

The C_v parameter is a modified drag coefficient, calculated as:

$$C_v = MIN\left[3.5 + \frac{73.14}{Re^{0.264}} + \frac{2.79 \cdot 10^{10}}{Re^{279}}, \frac{2.6}{\varepsilon^2}\right]$$

The fuel pin simulator is reproduced with a single equivalent channel, axially divided into an appropriate number of volumes to individuate the FPS main regions and to compare the calculated LBE temperature in the correct TCs axial positions: 3 volumes for the bottom mixing zone (in yellow), 8 for the active length (in red) and 5 for the top mixing zone (in yellow). The active region is thermal coupled with a heat structure reproducing the thermal power supplied by the 37 pins (80 active nodes), imposed with a general table as boundary condition. In addition, 60 passive thermal nodes simulate the heat dissipations through the FPS hexagonal shell, considering an equivalent cylindrical geometry in which the inner and outer diameters are calculated to preserve the thermal inertia of the hexagonal duct, and the active length of each heat structure is evaluated to obtain the correct heat exchange area. R5-3D includes two correlations for the evaluation of the liquid metal heat transfer coefficient (HTC): for bundle and non-bundle geometries. In bundle geometry, the HTC is evaluated with the Westinghouse correlation (The RELAP5-3D© Code Development Team, 2015b):

$$Nu = 4.0 + 0.33\left(\frac{p}{d}\right)^{3.8}\left(\frac{Pe}{100}\right)^{0.86} + 0.16\left(\frac{p}{d}\right)^{5}$$

where *Pe* represents the Peclet number. The correlation was obtained in the ranges of 1.1<*p/d*<1.4 and 10<*Pe*<5000; this means that FPS p/d is out of validity range. In addition, Westinghouse correlation underestimates the HTC for *p/d* higher than 1.2 (Kazimi and Carelli, 1976). According to the state of art, an HTC better estimation was found with Ushakov correlation (Ushakov et al., 1977):

$$Nu = 7.55\frac{p}{d} - 20\left(\frac{p}{d}\right)^{-13} + \frac{3.67}{\left(90\frac{p}{d}\right)^2} Pe^{\left(0.56+0.19\frac{p}{d}\right)}$$

In CIRCE-ICE operational temperature and velocity, the two correlations show a similar gradient of *Nu* versus *Pe*; for this reason, it is possible to calculate a constant value of the ratio between Ushakov and Westinghouse correlations, equal to 1.2. This multiplicative

factor has been applied to the LBE side HTC of the FPS active heat structure as described in Giannetti et al. (2016).

For non-bundle geometry, Seban-Shimazaki correlation is applied (The RELAP5-3D© Code Development Team, 2015b):

$$Nu = 5.0 + 0.025Pe^{0.8}$$

A vertical pipe is used to model the connection between the HS and the fitting volume. The not insulated walls of this component, allows a large amount of heat losses towards the pool, playing a relevant role in thermal stratification. A sensitivity study was carried out modelling the fitting volume with a single volume and with a horizontal pipe with variable flow area (in green in Fig. 4). The analysis highlighted that the second approach allows a better simulation of the flow path inside the component, providing an improved evaluation of the heat transfer coefficient. As presented in Narcisi et al. (2017), a single volume cannot reproduce the LBE flow condition within the fitting volume, underestimating the HTC inside the component. This causes a large underprediction of the temperature in the middle of the pool, failing to reproduce the qualitative temperature profile. The riser (in blue) is modelled with a vertical pipe composed of 26 control volumes. The gas lift system is simulated with a time-dependent junction, connected with the bottom of the riser, which sets the argon flow rate injected inside the test section; the gas conditions are defined with a time-dependent volume. In the upper part, the separator operates as a hot pool, allowing the separation of the two phases. Due to the large difference in density between molten LBE and argon, the fluctuation of the free surface produces oscillations in the LBE mass flow rate calculated by R5-3D. A sensitivity study was performed on the separator modelling approach in order to reduce the mass flow spikes. Different methods were investigated: a single vertical pipe, two, three and four parallel vertical pipes with cross junctions, and a MULTID component. The analysis highlighted that a single pipe allows to dump the large oscillations of the primary mass flow rate, but this approach cannot reproduce the fast free level decrease occurring in the first seconds after the transition from GEC to NC. Using multiple parallel pipes with cross junctions, the buoyancy inside the large component is better simulated, allowing the free surface movement. However, this solution causes mass flow fluctuations when the free level passes through two contiguous volumes; the oscillations increase with the number of parallel pipes and adopting the MULTID component. For this reason, two parallel pipes with cross junctions were adopted and the effect of the axial meshing was assessed, highlighting that a coarse vertical division reduces the mass flow spikes, limiting

the free level passage between contiguous volumes. The separator is connected upward with the gas plenum, composed of a vertical pipe where the cover gas pressure is fixed by a time-dependent volume above the pipe, and downward with the HX. The primary side of the heat exchanger is modelled with a single equivalent pipe composed of 22 control volumes (in orange), reproducing the HX sub-channels. On the secondary side, the 91 bayonet tubes are represented with two equivalent tubes, modelling the descending and the ascending side of the bayonet element (in yellow). Two time-dependent volumes impose the FW inlet temperature and the mixture outlet pressure, and the secondary mass flow rate is set by a time-dependent junction. The HX primary and secondary sides are thermally coupled with 1054 heat transfer nodes. As described for the HS bundle, for the evaluation of the LBE side HTC, a multiplicative factor, equal to 1.02, is applied. In addition, 310 thermal nodes simulate the heat exchange between the descending and the ascending secondary side and other 230 reproduce the heat losses between the HX and the LBE pool.

The DHR is immersed inside the pool; its modelling (in red) consists of a single pipe for the LBE side and two pipes for the secondary side. Two time-dependent volumes set the air inlet temperature and the outlet pressure, and a time-dependent junction imposes the air mass flow rate. Three heat structures reproduce the heat removed by the system, the heat losses towards the pool and the heat exchange between the descending and the ascending secondary side.

As reported in section 1, multiple channels with crossflow junctions are needed to reproduce multi-dimensional flow effects in large pools. The presence of the cross junction in each volume does not allow the application of the R5-3D thermal stratification model and a detailed axial discretization is required for the evaluation of phenomena such as thermal stratification. For this purpose, CIRCE pool is modelled with three parallel pipes, dividing the tank into three sections as shown in Fig. 5. Each pipe is divided in 52 control volumes. The axial mesh sizing follows the flow path nodalization, according with the sliced modelling approach and the vertical stratification model is applied in all the vertically oriented volumes. Furthermore, this geometrical scheme allows the comparison of the calculated LBE temperature in the correct axial positions of the TCs installed inside the pool.

In a large pool, the liquid is free to flow in all directions, depending on the pressure gradient. In order to reproduce the horizontal flow, 156 cross junctions connect adjacent volumes at same axial levels. The junction area is equal to the flow area in the cross direction per each

level. The pressure gradient between adjacent pipes is calculated by R5-3D; no form loss coefficients are included in the cross junctions modelling.

The heat losses from the primary flow path are completely simulated. Moreover, the heat dissipations through the vessel walls are considered assuming a constant temperature of the external environment and imposing a constant HTC on the outer wall of the insulator.

Mesh and time step sensitivities were carried out. The mesh sensitivity analyzed the effect of FPS, riser and HX axial discretization on the accuracy of the solution. Three calculations were performed, assuming control volumes mean length equal to 0.1, 0.15 and 0.2 m, highlighting negligible differences. The results of the study will be presented in section 5. About the pool, Ahn et al. (2018) highlighted that the effect of the axial discretization on the accuracy of solution is minimal and a sufficiently fine meshing permits a good evaluation of the thermal stratification. For this purpose, CIRCE-ICE model presents a very fine nodalization along the axial coordinate, following the primary flow path discretization, according with the sliced modelling approach.

The time step sensitivity study was carried out assuming three different values of the maximum time step size: 0.005, 0.002 and 0.001 s. Negligible effects were highlighted proving that this parameter does not affect the accuracy of the results. The analysis will be presented in section 5.

The second geometrical scheme (model #2) aims to investigate more accurately the fuel pin simulator and the pool. The main primary flow path is the same of the previous nodalization, except for the FPS, that is reproduced with all the actual sub-channels, and the pool, in which a multi-dimensional component substitutes for the three parallel pipes.

Fig. 6 shows the scheme of the HS modelling. The whole model consists of 72 parallel channels reproduced with pipe components. Three different channel type are defined: inner subchannels (54), edge subchannels (6) and corner subchannels (12). Each subchannel maintains the axial division presented in model #1 but the flow area and the equivalent diameter has been evaluated considering the geometry presented in Fig. 6. As described in Memmott (2010), cross flow represents a crucial aspect for the correct evaluation of the coolant temperature. Cross flow depends on the pressure gradients between adjacent subchannels, and on the hydraulic resistance. In order to evaluate the mass transfer between subchannels, 1536 cross junctions are included in the FPS modelling, connecting adjacent subchannels for each axial level. Junction area is calculated as the lateral flow area

between two adjacent pins for each level. The pressure gradient is evaluated by RELAP5-3D, while the hydraulic resistance is introduced as a local pressure loss coefficient depending on flow regimes. Idelchik (1986) equation for the calculation of the form loss *K* for bundle of staggered rods was used:

$$K = \left(z_p + 1\right) \cdot A \cdot \varphi \cdot Re^{-0.27}$$

where *A* is evaluated as:

$$A = 3.2 + 0.66a_1$$

$$a_1 = (1.7 - \bar{s})^{1.5}$$

For FPS bundle geometry, φ and $\bar{s}$ are equal to 1. According with this equation, the form loss coefficients, dependent on flow conditions, are introduced in the model as:

$$K = 7.17 \cdot Re^{-0.27}$$

The thermal power, provided by the electrical heated pins, is reproduced with 5760 heat transfer active nodes, supplying the power proportional to the heat transfer area of the control volumes that compose the active zone. As for the model #1, a multiplicative factor is applied to the active heat structure to better reproduce the HTC, according to the Ushakov correlation. According with the experiment, the power distribution is considered flat. In addition, 1728 passive thermal nodes reproduce the heat dissipation through the hexagonal shell, coupling edge and corner sub-channels with the volume between the hexagonal and the cylindrical shells.

In section 5, the thermal conduction effect between adjacent subchannels is analyzed. At full power operation the conduction effect is negligible but, at low mass flow rate (typically in natural circulation condition), thermal conduction must be considered. For this purpose, 3456 heat structure nodes simulate the heat transfer between adjacent sub-channels, assuming a dummy material with negligible heat capacity and the LBE thermal conductivity. A high HTC multiplicative factor is applied to practically exclude the convective resistance on the evaluation of the heat transfer.

The second improvement, introduced into the model #2, is the MULTID component, which simulates the pool of the facility (see Fig. 7). The model consists of 4 radial meshes (r-coordinate), 8 azimuthal intervals (theta- coordinate) and 51 axial levels (z- coordinate). Nodalization scheme in r- and theta- directions is highly dependent on the test section

asymmetry, as shown in Fig. 7 where cross section at 7 relevant axial levels are reported showing the volume occupied by the internals, and the TCs positioning, seen in Fig. 2. According with the sliced approach, the nodalization along the z- direction follows the mono-dimensional mesh of the primary flow path. This allows the comparison of the LBE temperature in the “real” position of the thermocouples. Volume factors, defined as the ratio between the real free volume and the mesh original volume, are introduced to consider the volume occupied by the test section. In the same way, junction area factors are calculated for the flow area evaluation in three directions. In order to limit the wall friction in free volumes inside the MULTID component, a high equivalent diameter is introduced when fluid is free to move without interaction with walls.

The whole heat losses between test section and LBE pool are considered. Several heat structures are introduced, coupling each component of the 1D model with the correct pool zone. In addition, the heat losses towards the external environment are considered, applying the same boundary conditions of model #1.

Models dimensions and relative calculation times are summarized in Tab. 2. The calculation time is related to a single core of an Intel® Xeon® E5-2690 v4 @3.22 GHz used in both calculations, adopting a time step equal to 0.005 s for the calculations.

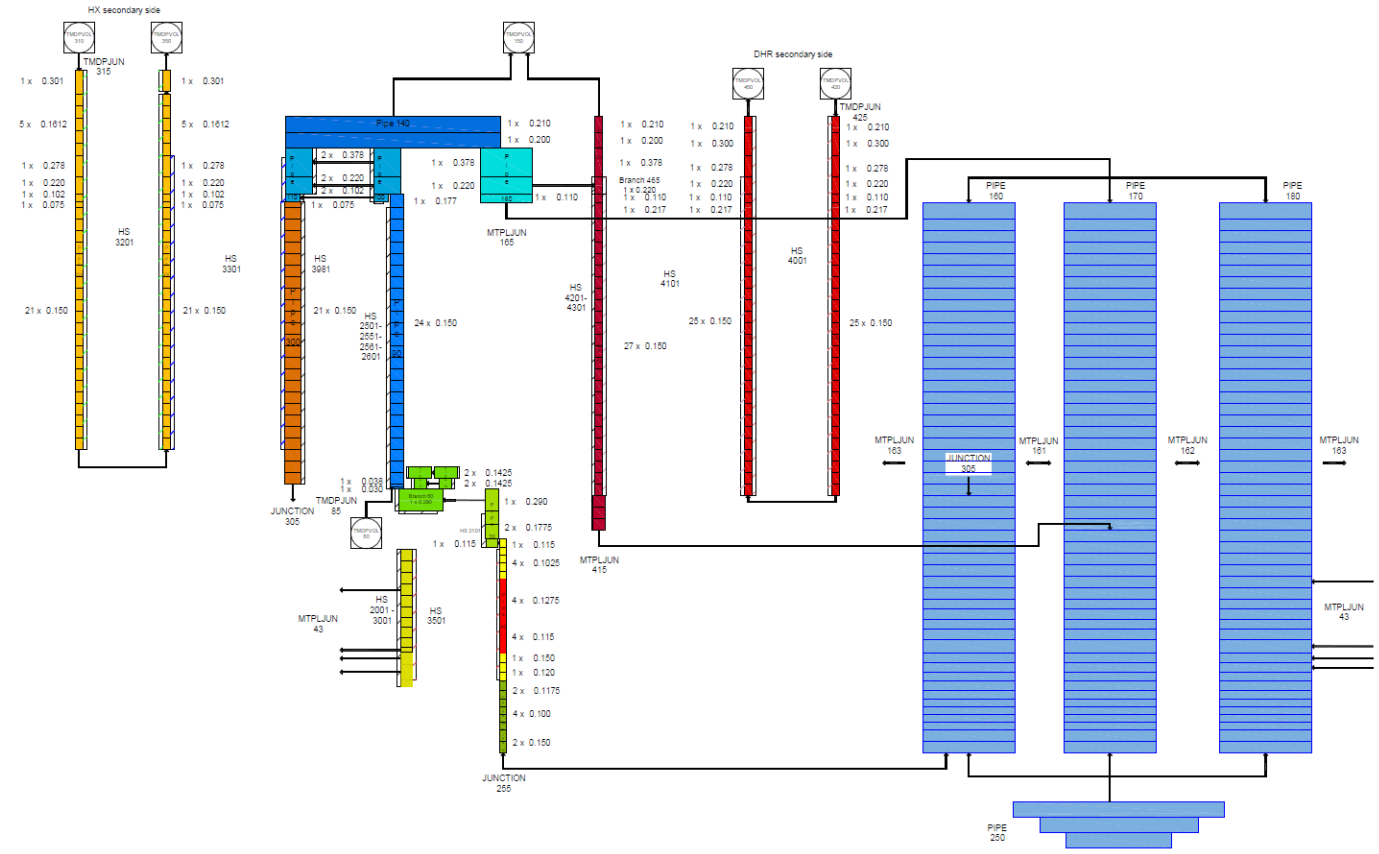

Fig. 4. CIRCE-ICE nodalization scheme: model #1

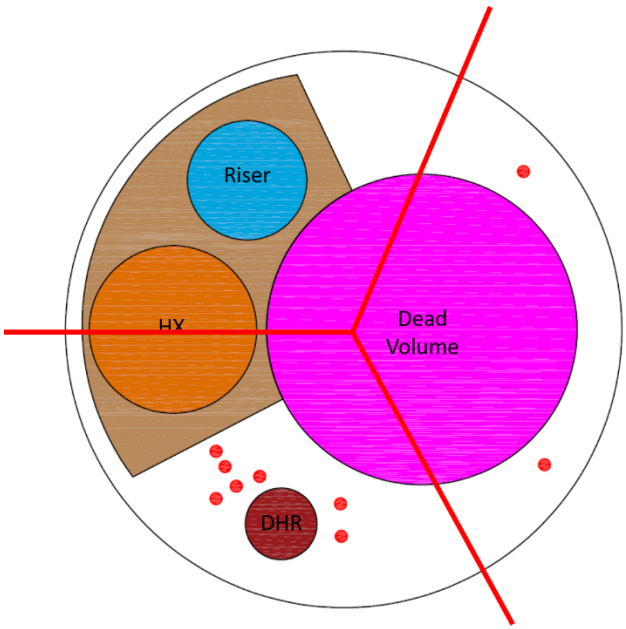

Fig. 5. Pool nodalization approach: model #1

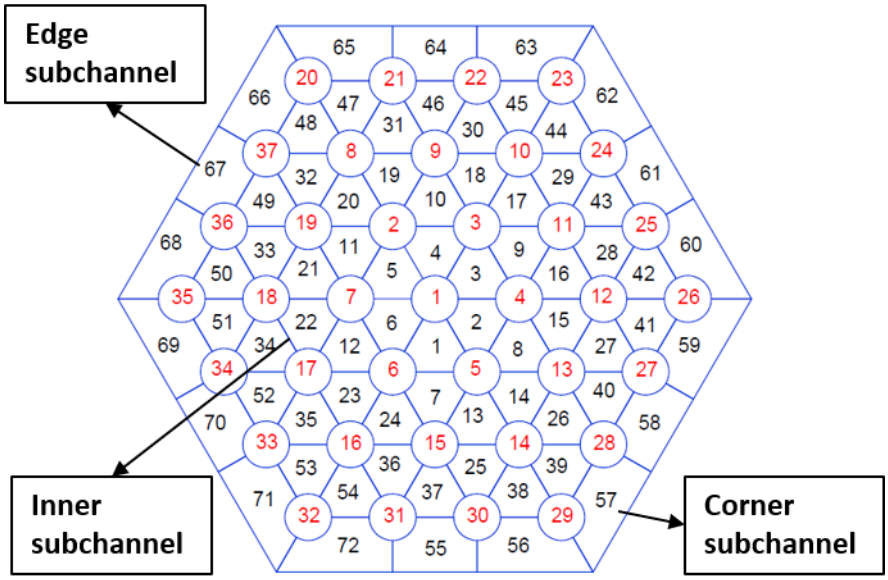

Fig. 6. FPS nodalization scheme: model #2

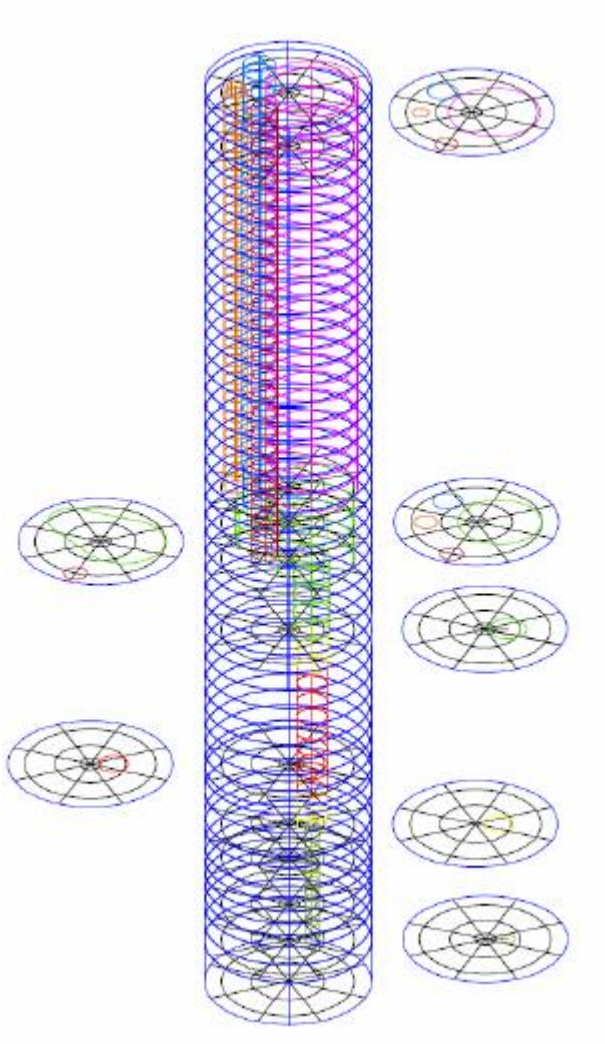

Fig. 7. MULTID component: model #2

Parameters	Model #1	Model #2
Number of hydrodynamic volumes	355	1929
Number of hydrodynamic junctions	409	4856
Number of heat structure mesh points	3828	15353
Mean calculation time (CPU time / problem time)	8.5	60

Tab. 2. Models #1 and #2: main parameters

4. Simulations results

All the calculations analyzed in this section have been performed using the most recent LBE thermophysical properties correlations, recommended by NEA (OECD/NEA Nuclear Science Committee, 2015) and implemented in R5-3D, as shown in Balestra et al., 2016. Concerning the MULTID component, the three-dimensional momentum equations are used.

4.1 TEST A

Boundary conditions, described in section 2.2, are shown in Fig. 8, where the reproduced values have been compared with the experimental data. The test starts at no-power steady state conditions. Fig. 8 (a) and (c) show that, at the beginning, the experimental measurement system acquires non-zero value for argon and feed-water flow rate (0.35 Nl/s and 0.1 kg/s respectively), due to the instruments signals, which are at digital full scale. For this reason, the simulated inlet flows are set to zero. When Ar injection system is activated, the reproduced value increases to the nominal flow rate, neglecting the peak during the first minutes of the transient.

Fig. 8 (b) compares the experimental electrical power supplied to the FPS with the simulated HS thermal power. According to Bandini et al. (2015), the simulated value has been reduced to 95% of the nominal power, taking into account the dissipations which occur in the cables and connectors of the outer circuits, that do not contribute to the thermal power supplied to the primary coolant. The thermal power provided to LBE is equal to Joule heat production along the nickel chrome wires that compose the FPS active length (Tarantino et al., 2015). The amount of the dissipations in the cables of the outer circuits has been estimated from the circuit length and electrical resistivity.

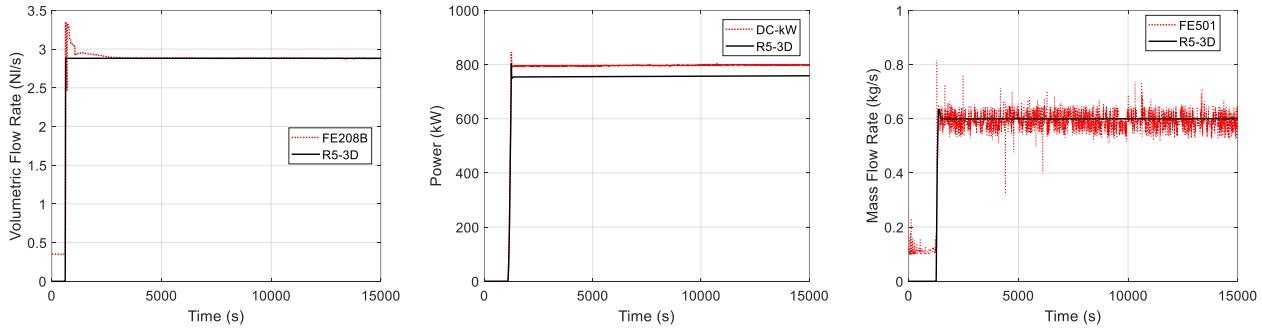

(a) Ar injection (b) FPS Power (c) FW mass flow rate

Fig. 8. TEST A: Boundary conditions

In next figures, simulation results are compared with experimental data, which are reported with their uncertainties bands (dotted line). The experimental data have been smoothed with Savitzky-Golay filter (Press and Teukolsky, 1990). The standard deviation of the measurements has been included in the global uncertainties, as proposed by Martelli et al., 2015.

In Fig. 9, the LBE mass flow rate acquired by the flow meter (FM), reported in red line, is compared with the flow rate predicted by the two models in the actual position of the

instrument. After the activation of Ar injection system, the primary mass flow rate reaches a value of 62 kg/s, maintained until the heater activation, which occurs at 1100 s. At this point, the mass flow increases up to 65 kg/s, due to the natural circulation (NC) contribution. As shown in Fig. 9, the models provide a good estimation of the LBE flow rate, in both gas enhanced (GEC) and gas enhanced plus natural circulation (GEC+NC), proving the capability of the two geometrical schemes to reproduce the argon-induced natural circulation and the pressure drops of the whole primary system at high values of the Re number. After the FPS activation, adopting the model #1, an oscillation of the LBE mass flow is highlighted, due to the instantaneous NC contribution, that is damped down in 2000 seconds. This phenomenon is not predicted by the model #2, which allows the mass transfer between the HS sub-channels, providing an instantaneous attenuation of the effect.

Fig. 10 compares the LBE temperature measured by the TCs at the HS inlet and outlet with the simulated values. At the FPS inlet, the liquid metal temperature is uniform; for this reason, the calculated values are compared with a single experimental data. At the active length outlet, experiment highlights significant non-uniform distribution of the temperature due to the larger LBE mass flow in the edge and corner subchannels, because of a larger flow area. In addition, heat losses through the hexagonal shell enhance this difference.

Temperatures acquired by two thermocouples at the HS outlet (T-FPS 34 and T-FPS-36) are reported. As exposed in section 3, the FPS nodalization scheme in model #1 consists in a single equivalent channel providing an estimation of the mean temperature at the HS outlet. Model #2 has been developed to carried out a subchannel analysis, so in Fig. 10, the experimental data are compared with the calculated temperature in the exact sub-channels (number 12 and 67 in Fig. 6). Both the models provide a good prediction of the qualitative temperature trends. In particular, model #2 reproduces very well the radial temperature distribution at the active length outlet, proving good capabilities of R5-3D to perform a subchannel analysis in LBE systems. The influence of the thermal conductivity will be presented in section 5.

Fig. 11 shows the comparison of the inlet and outlet HX primary side temperature. The temperature difference between HX inlet and FPS outlet provides an evaluation of the heat losses towards the pool. The higher heat dissipations occur inside the fitting volume and the separator, characterized by large not insulated walls. The qualitative trend of the HX inlet temperature is well reproduced by the two nodalization schemes, even if model #1 provides a larger estimation of the heat losses through the main flow path walls, underestimating of

5 K the HX inlet temperature, outside the lower limit of the error band. This can be explained by the underestimation of the pool temperature.

A comprehensive analysis of the pool thermal-hydraulics will be presented in the following. The temperature drop along the HX is well reproduced by both the models; Fig. 11 shows a lower value of the outlet temperature from the experiment but the discrepancy is justified by a not perfect positioning of the outlet control volume, which provides temperature calculation slightly upstream the TCs. The thermal power removed by the HX is compared in Fig. 12 and it highlights the good agreement of both simulations.

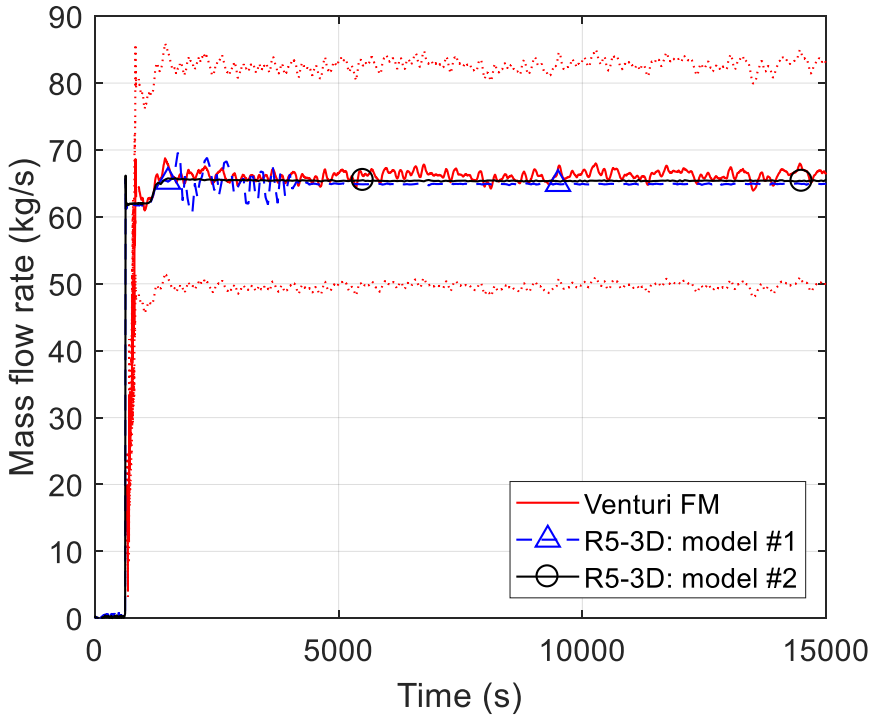

Fig. 9. TEST A: LBE mass flow rate

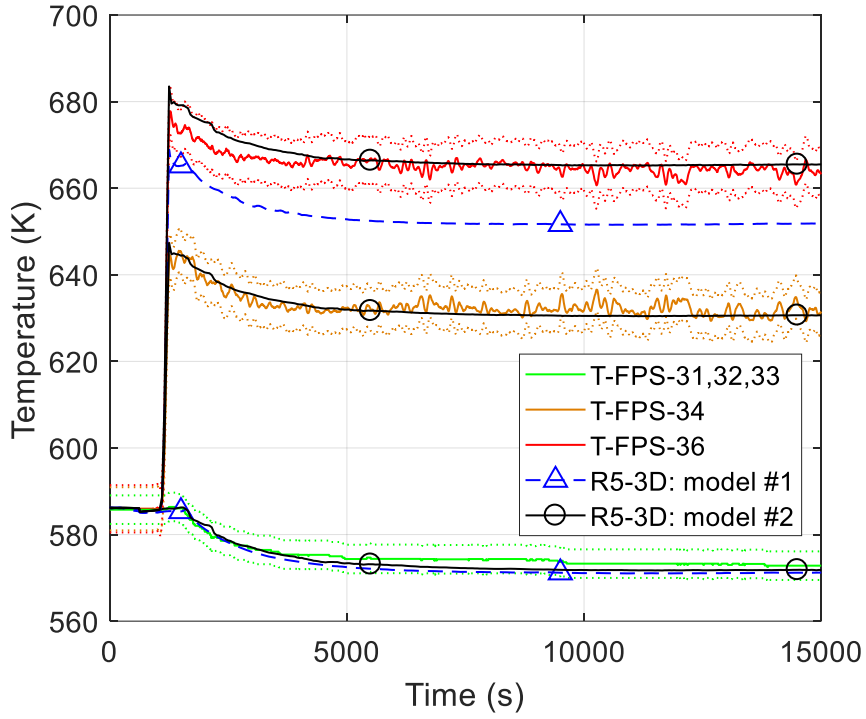

Fig. 10. TEST A: LBE FPS inlet/outlet temperature

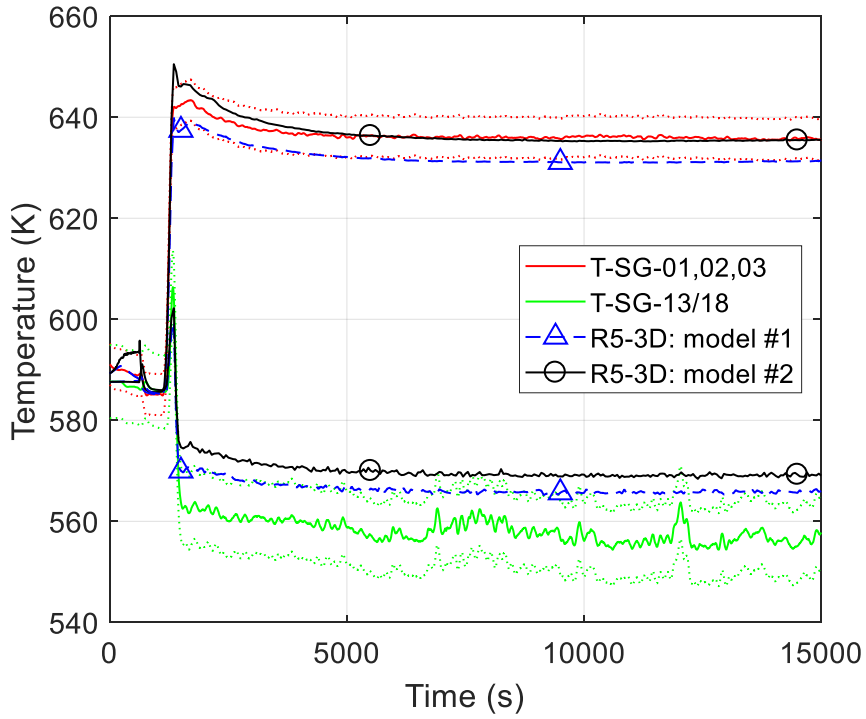

Fig. 11. TEST A: LBE HX inlet/outlet temperature

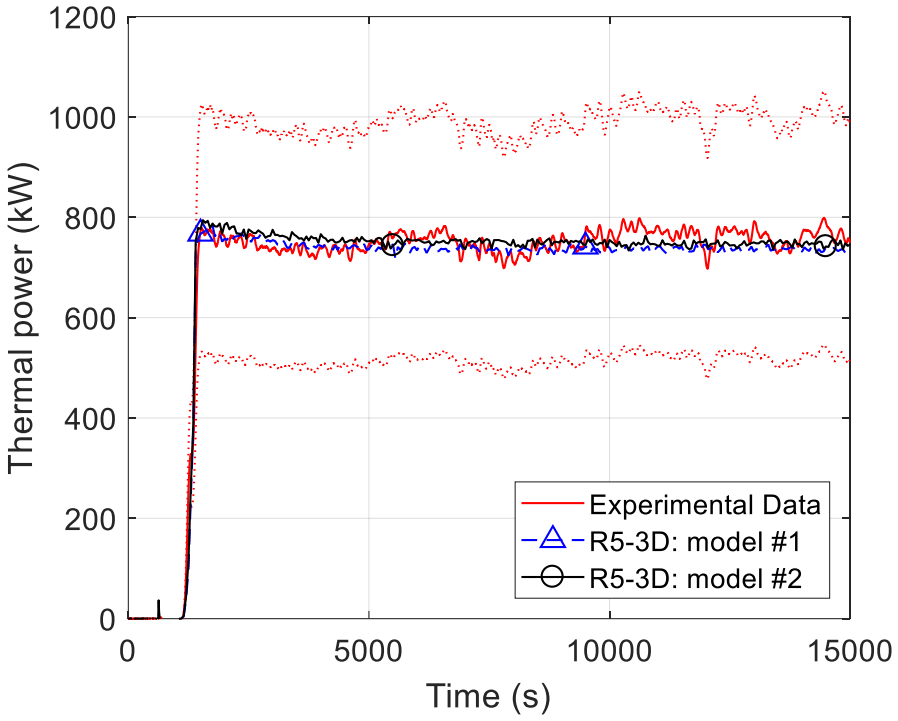

Fig. 12. TEST A: HX power removed

The next figures aim to evaluate the capability of R5-3D to reproduce the thermal-hydraulics of an HLM pool, adopting two different modelling approaches: a mono-dimensional model, consisting of three parallel pipes and several cross junctions, and a three-dimensional model, using a MULTID component to reproduce the large volumes and adopting three-dimensional momentum equations.

The vertical profile of the LBE temperature is analyzed in four relevant regions: Fig. 13(a) shows the mean value of the measurement in A, B, C, D and E positions, Fig. 13(b) represents the mean temperature acquired by TCs in F and G positions covering the upper part of the pool only and Fig. 13(c) and (d) show the LBE temperature along the H and I supports. In each figure, the error bar is associated to the experimental temperature.

Due to the pool modelling approach in model #1, the temperature trend is the same from Fig. 13 (a) to (d), whereas MULTID component in model #2 compares the effective temperature in the four relevant positions.

Experimental data show that at the same axial level LBE temperature is quite uniform while, in the vertical trend, two main stratification phenomena occur at the level of the HX, between 7 to 5.2 m, and of the fitting volume, between 3.5 and 4 m. The heat exchanger is not insulated and the external shell provides a large heat transfer area, cooling the LBE inside

the pool. This vertical trend is interrupted at the fitting volume level, where LBE temperature assumes a rather constant value of 592 K. The LBE inside the fitting volume, at about 660 K, warms the liquid metal in the pool, causing this temperature profile. Below the fitting volume, a steep stratification of 20 K occurs and, from 3 m to the lower plenum, the LBE assumes a uniform temperature of 570 K. Fig. 13 shows good capability of the two model to reproduce the qualitative temperature trend. Both the models are able to predict the two relevant thermal stratifications which occur inside the pool, even if some discrepancies are highlighted. The mono-dimensional modelling approach evaluates well the temperature in the lower part of the pool. Here the LBE temperature is a bit underestimated but discrepancy with experiment is limited within the error band (lower than 3 K). Thanks to the detailed nodalization along the vertical coordinate, the level of the middle stratification is well reproduced (4 m), even if a sharper temperature decrease is predicted. The maximum discrepancy with experimental data is observed between 4 and 6 m. In this zone, the magnitude of the temperature plateau is underestimated of about 15 degrees. The difference between experiment and calculations is reduced with the increase in the level, due to an over-prediction of the upper stratification slope.

The three-dimensional modelling approach highlights some improvements on the pool thermal-hydraulics evaluation. According with the experimental data, the MULTID component predicts a uniform temperature at the same level of the pool. The temperature in the lower volumes perfectly matches the measured values. Even if the magnitude of the temperature plateau between 3.5 to 5.5 m is underpredicted, the 3D nodalization, in comparison with model #1, provides a better estimation of the stratification slope between 3.5 and 4 m. The stratification level of 4 m is very well reproduced and the discrepancies with experimental data are reduced to about 12 K, although they are still higher than the upper limit of the error bands. The overprediction of the heat losses along the hot leg, previously discussed, could be explained by the higher discrepancies observed within the pool by model #1.

Fig. 14(a) shows the LBE temperature obtained in the MULTID component, observing the most representative section that includes the FPS and the HX. To provide useful qualitative information, the DHR element is also included in the section. The temperature map shows that the upper stratification occurs in the first half of the HX, following the temperature drop along this component. Between 5.5 to 4 m, the temperature is quite uniform and then the second stratification occurs at the fitting volume level. Fig. 14(b) shows the error distribution

map in the same section. The TCs cover only 9 positions in the r-theta plane so, to obtain the experimental data map, uniform temperature is considered at the same levels (the experimental results justified this assumption) and along the z- coordinate, the LBE temperature is obtained with linear interpolation between two consecutive measurement points, in order to cover the whole axial length. The picture highlights that the three-dimensional model provides a perfect matching in the lower half pool. The error sharply increases at 4 m and it is maintained higher than 10 degrees up to the gas plenum (the maximum discrepancy of 13 K occurs at about 6 m). The large discrepancy at the HX outlet is not representative because it is expected that in this point the temperature is lower due to the cold LBE exiting the HX and it is not possible to consider uniform temperature in this region.

These results highlight the limits of RELAP5-3D to reproduce the exact temperature trend in a large HLM volume. In fact, R5-3D provides only one HTC correlation for HLM in a non-bundle geometry, mainly developed for liquid metal flowing in a duct. A situation where the liquid metal is in a quasi-stagnant condition in a large volume, is out of the applicable range of the Seban-Shimazaki correlation, and the constant term included in this correlation could underestimate the heat transfer. In addition, R5-3D have not a fully integrated heat conduction model for the working fluid and this term could assume relevant role in HLM systems (the effect of liquid thermal conduction is evaluated in the section 5).

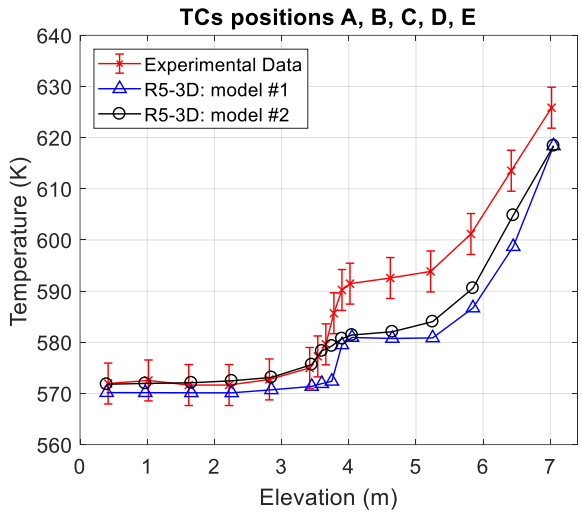

(a)

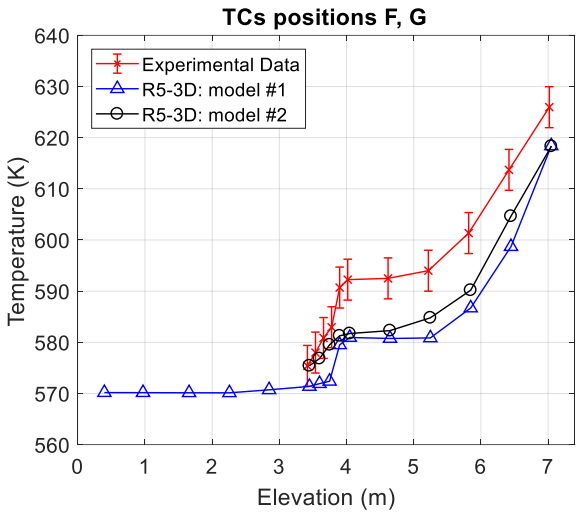

(b)

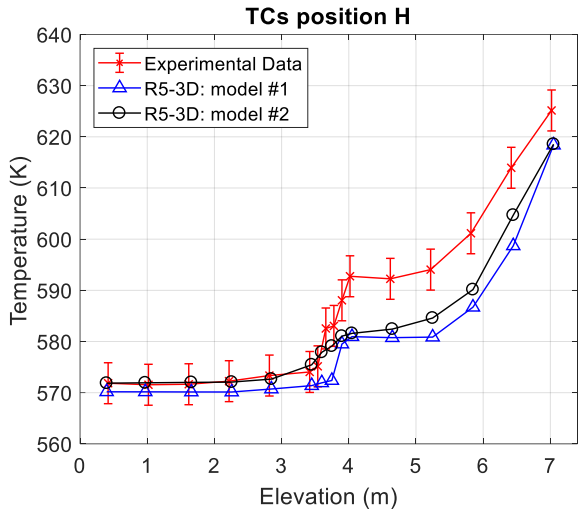

(c)

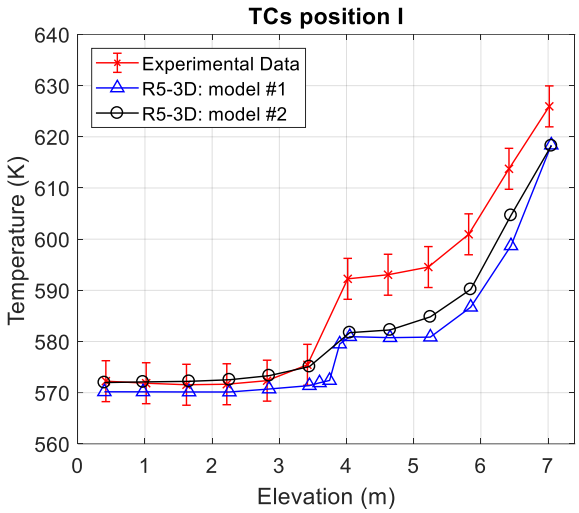

(d)

Fig. 13. TEST A: pool thermal stratification

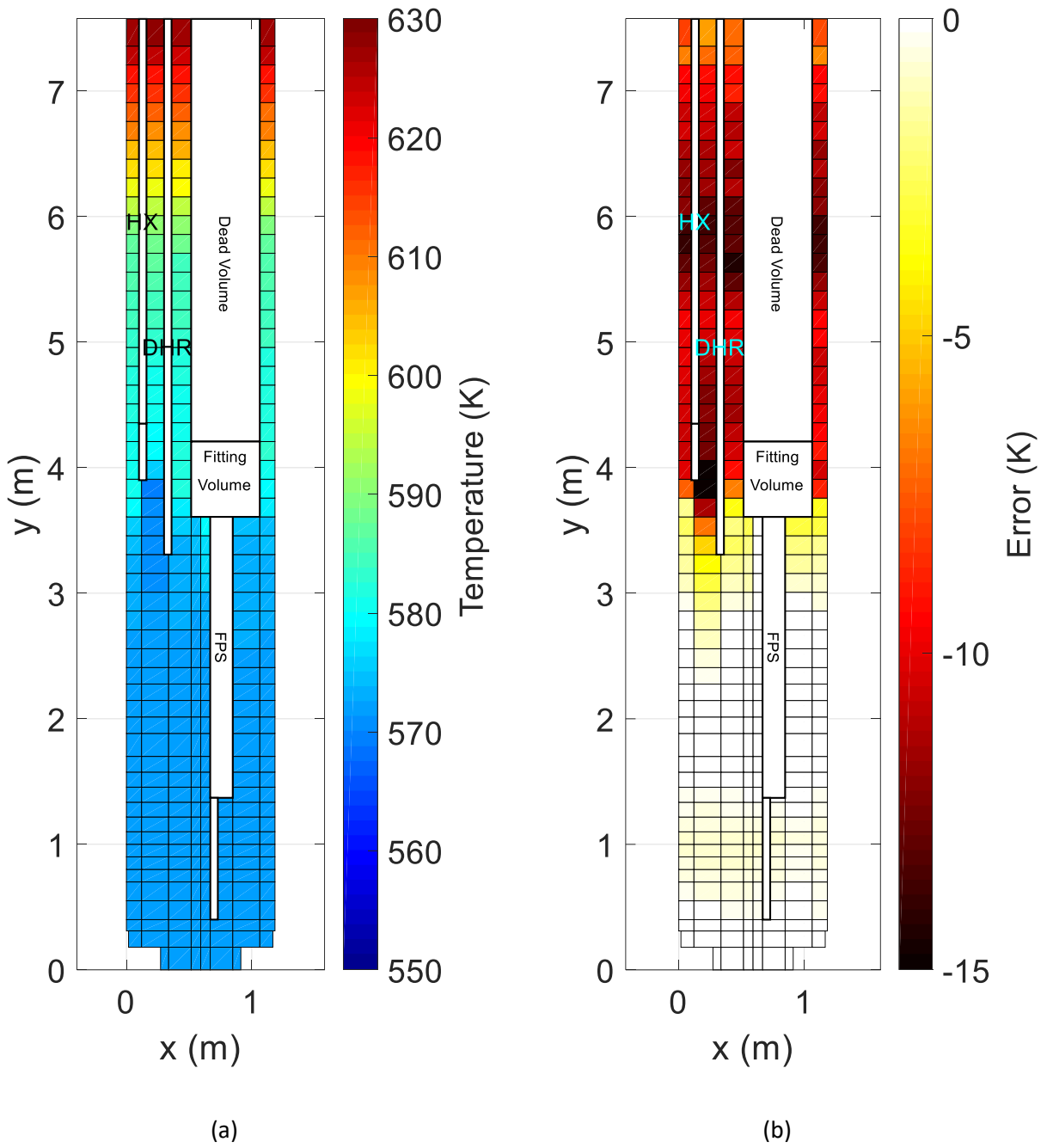

Fig. 14. TEST A: pool temperature, model #2

4.2 TEST I

Test I has been reproduced to verify R5-3D capability to simulate a transition from GEC to NC with activation of DHR system. The boundary conditions assumed for the calculation are presented in Fig. 15. The test starts at zero-power steady state conditions, with each control system turned off. After 450 s, argon is injected inside the test section with a volumetric flow rate of 1.7 Nl/s, increasing to 1.78 at 8600 s. At 25400 s the gas injection is disabled, decreasing to zero in 1 second (the instruments signal reaches the digital full scale at 0.35

Nl/s in Fig. 15(a)). The FPS power ramp (see Fig. 15 (b)) starts at 920 s, reaching the nominal value after 180 seconds; full power conditions are assumed with a 5% reduction of the electrical signal to consider dissipations. At 25300 the transient event starts and the power is reduced to 7% in 130 s. Feed-water injection is depicted in Fig. 15 (c) and it is replaced in R5-3D, unless the fluctuation due to the measurement chain. Fig. 15 (d) shows the air mass flow rate that feeds the DHR system; at the beginning, the measurement of the air flow rate is disabled, giving a value of zero but the control system set the air mass flow in order to remove about 3 kW. For this reason, a mass flow rate of about 21 g/s is considered in the calculation, for the first part of the test. After the transition from GEC to NC, the air flow rate is increased following the experimental curve and setting a constant value of 226.7 g/s.

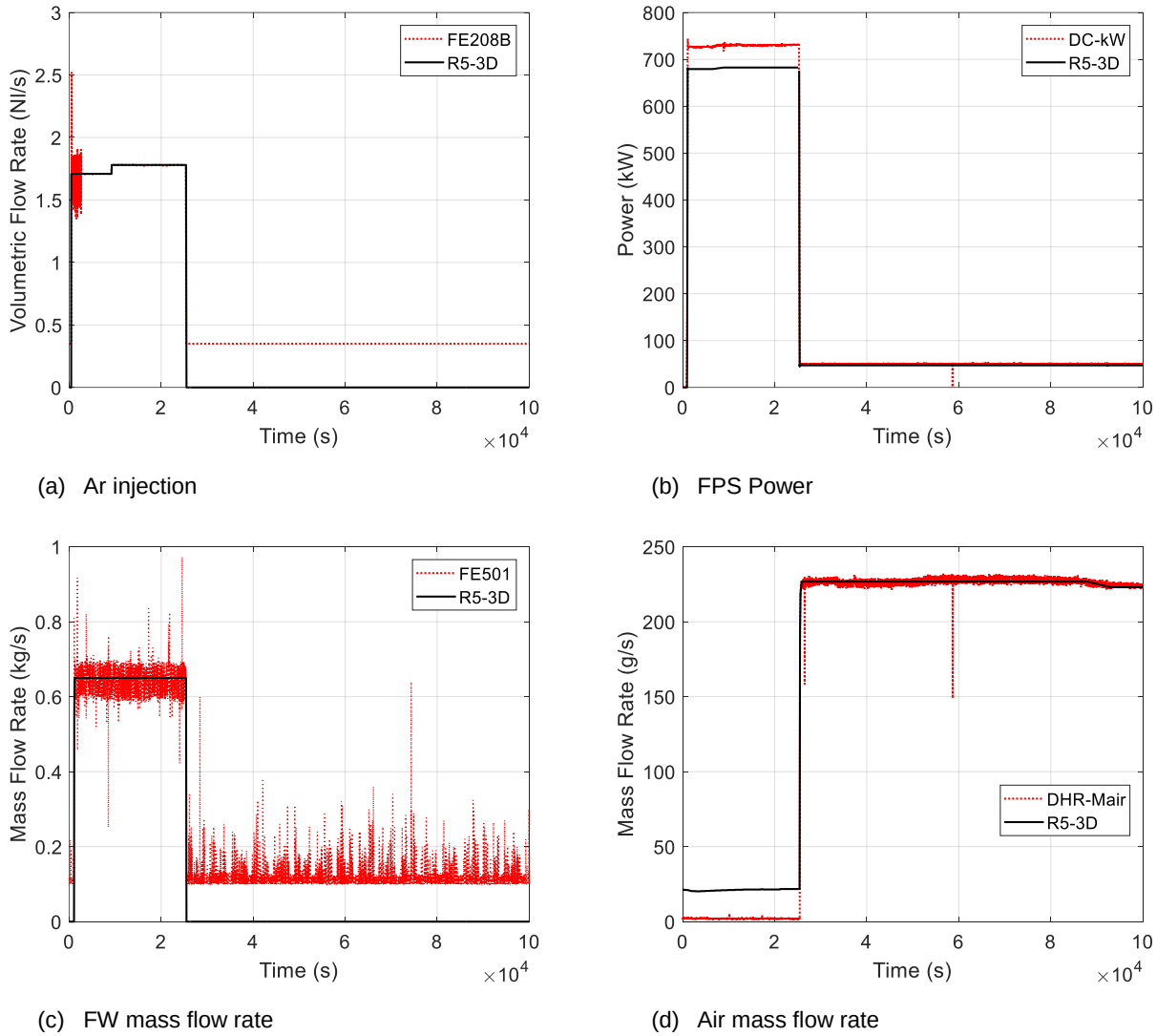

(a) Ar injection

(b) FPS Power

(c) FW mass flow rate

(d) Air mass flow rate

Fig. 15. TEST I: Boundary conditions

Fig. 16 compares LBE mass flow rate acquired by Venturi FM with the values obtained by calculations. At full power conditions, the acquisition system observes a constant LBE flow

rate of 56 kg/s; after the transition, natural circulation is established to 7.3 kg/s. Both the calculations highlight a good prediction of the primary mass flow rate in GEC conditions. After the transition, both the simulations show a slight overestimation of the flow rate acquired by Venturi FM. At low values, the measurement system is affected by large uncertainties: that could explain these discrepancies; in fact, the mass flow rates evaluated by R5-3D (8.4 kg/s with model #1 and 8.6 kg/s with model #2) are included within the error bands. Natural circulation is mainly due to the thermal power supplied by the FPS and the heat losses towards the pool and the calculations demonstrate the R5-3D capabilities on the prediction of macroscopic phenomena during a postulated accident in an HLM system.

Fig. 17 shows the LBE temperature trend at inlet and outlet of the FPS active length. During the full power operation, the LBE temperature at the FPS inlet is uniform. The two models provide a good estimation of the temporal trend, highlighting a slight under-prediction of the temperature, even if the discrepancies are contained within the error band. At the HS outlet, model #1 evaluates a good qualitative trend of the mean temperature. The sub-channel analysis carried out with model #2, highlights code capability on the evaluation of the inner sub-channel temperature, acquired by the thermocouple T-FPS-36. However, the temperature on the edge subchannel is underestimated of about 6 degrees (T-FPS-34). The lack of information about the exact position of the thermocouple T-FPS-34 could explain this discrepancy. In fact, it is expected a quite uniform temperature in the inner subchannels, due to the uniform distribution of the thermal power, and a sharp decrease at the lateral edge. For this reason, the value of the temperature is strongly influenced by the exact position of the instrumentation. Unless this discrepancy, R5-3D shows enough capabilities on the utilization as a subchannel analysis code, providing estimation of the temperature difference between the center and the edge of the bundle.

During the first hour after the transition, both the models well reproduce the low peak at the HS inlet. Up to the end of the test, the models are able to simulate temperature evolution at the FPS inlet due to the global thermal power imbalance, limiting the discrepancies with experimental data within the error bands (lower than 3.6 degrees). At the HS outlet, the prompt temperature decrease is well predicted by R5-3D. Model #1 calculates a qualitative trend in good agreement with experimental data. After the transition from GEC to NC, the temperature difference between inner and edge subchannels is reduced, due to the low primary mass flow rate. The transition is well reproduced by model #2 that is able to predict

the temperature distribution inside the bundle. The discrepancies with experimental data are limited to a maximum value of 3.5 K at the end of the test.

Fig. 18 shows the comparison of the LBE temperature through the HX. The two models well reproduce the qualitative trend of the temperature over the whole test. As for TEST A, model #1 highlights higher heat losses through the hot leg, calculating a lower HX inlet temperature during the GEC operation (about 3 K). The peak temperature at 650 s is under-predicted by the calculations, even if the discrepancies with experimental data are contained within error bands. Some differences are observed in the first hour of the transition, when the prompt temperature decrease at the HX inlet is underestimated by the simulations. After that, the qualitative trend is well reproduced by the code, even if the two calculations provide slightly different results: the inlet temperature is over-predicted by model #1 of about 1 degree. After the loss of heat sink, the temperature drop provides information about the heat losses through the HX shell. The two simulations agree but, in comparison with experimental data, the temperature drop is under-predicted of about 1.8 K, proving the underestimation of the heat losses towards the pool. This sentence is confirmed by the power removed by HX, showed in Fig. 19. The experimental power is obtained applying the energy balance equation, considering the LBE temperature acquired by the TCs at HX inlet and outlet section and the LBE mass flow rate measured by the Venturi flow meter. For this purpose some assumptions are considered: the whole mass flow rate flowing through the hot leg is led into the HX and steady state conditions are supposed. The propagation errors have been calculated and reported in the figure as dotted line. Fig. 19 shows the over-prediction of the power removed by the HX but the large uncertainty bands make difficult the assessment of the calculation goodness.

The temperature evolution at the DHR inlet and outlet primary side is presented in Fig. 20. The large error band (+/- 17 K) at the DHR outlet are due to the high fluctuations that the acquisition of the TCs at the outlet section was affected. During GEC operation, the DHR system is turned off and the temperature difference between inlet and outlet is mainly due to the thermal stratification inside the pool, explaining the discrepancy of the outlet temperature calculated with model #1. After the simulated accident, the DHR is fed with air mass flow rate (see Fig. 15 (d)) and both the models provide a good estimation of the DHR behavior. The simulations highlight an overestimation of the intel temperature of about 3 degrees, remaining within the error bands. This behavior will be explained in the thermal stratification analysis. Unless this difference, the temperature drop across the DHR is well

reproduced by the two models, matching very well the LBE outlet temperature in NC operation. This is confirmed in Fig. 21, where the experimental power removed by the DHR is compared with R5-3D results. The prompt power increase is well predicted by the calculations that match well the experimental data until 80000 s. After that, experimental data assumes a lower gradient and the discrepancy with computational results increases up to 4% at the end of the test.

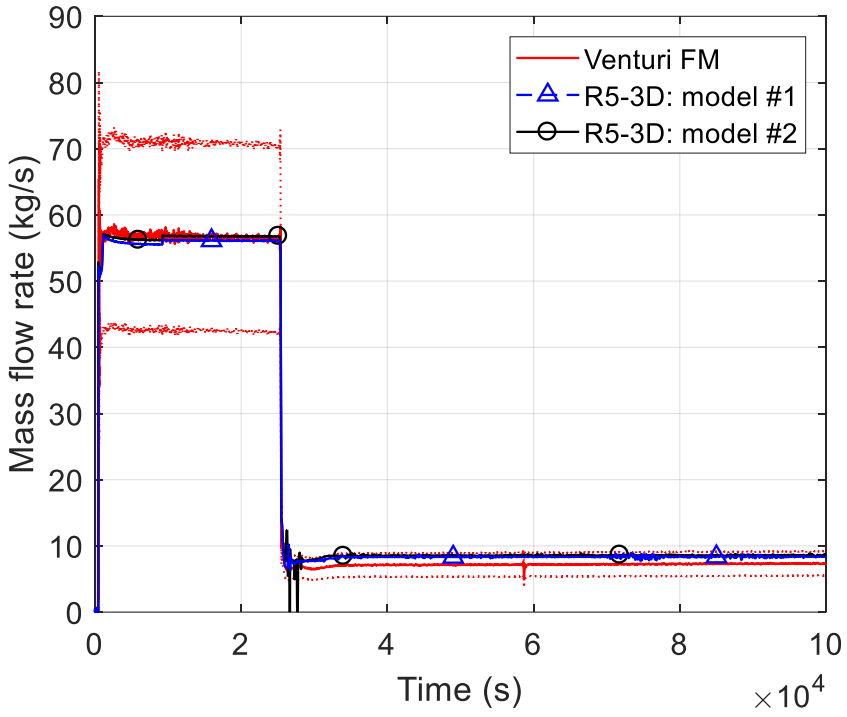

Fig. 16. TEST I: LBE mass flow rate

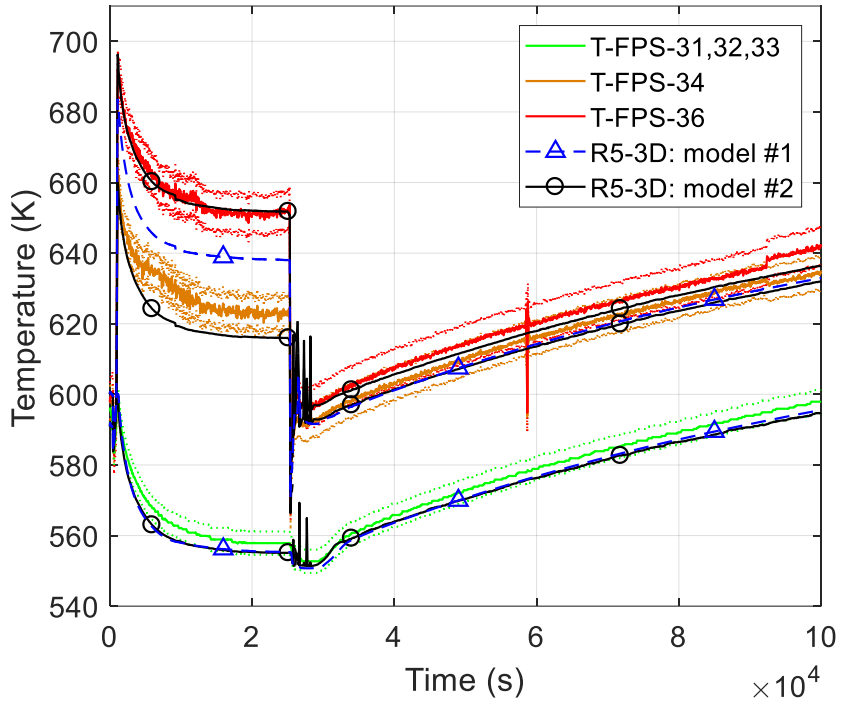

Fig. 17. TEST I: LBE FPS inlet/outlet temperature

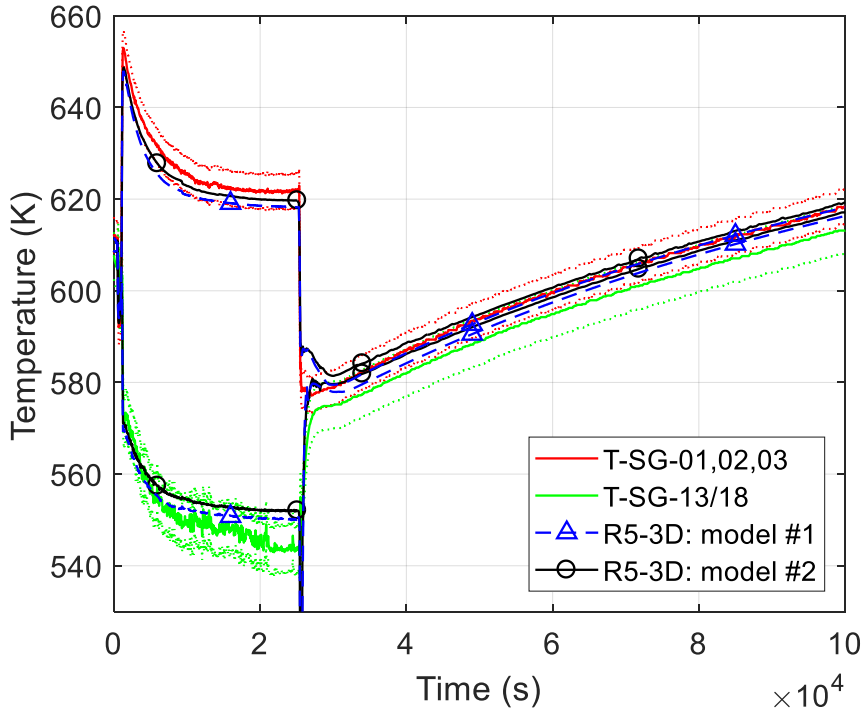

Fig. 18. TEST I: LBE HX inlet/outlet temperature

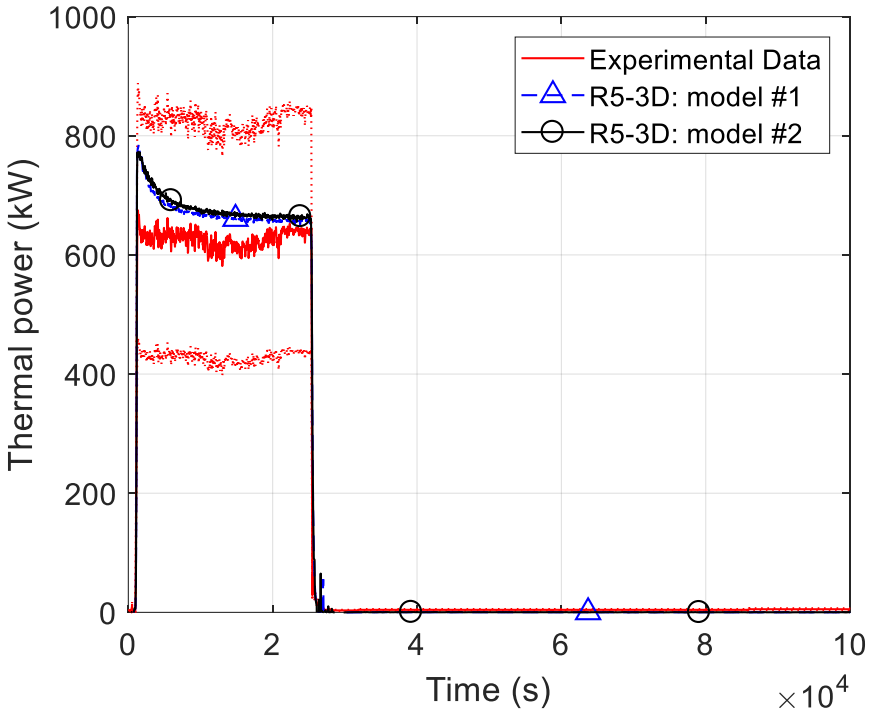

Fig. 19. TEST I: HX power removed

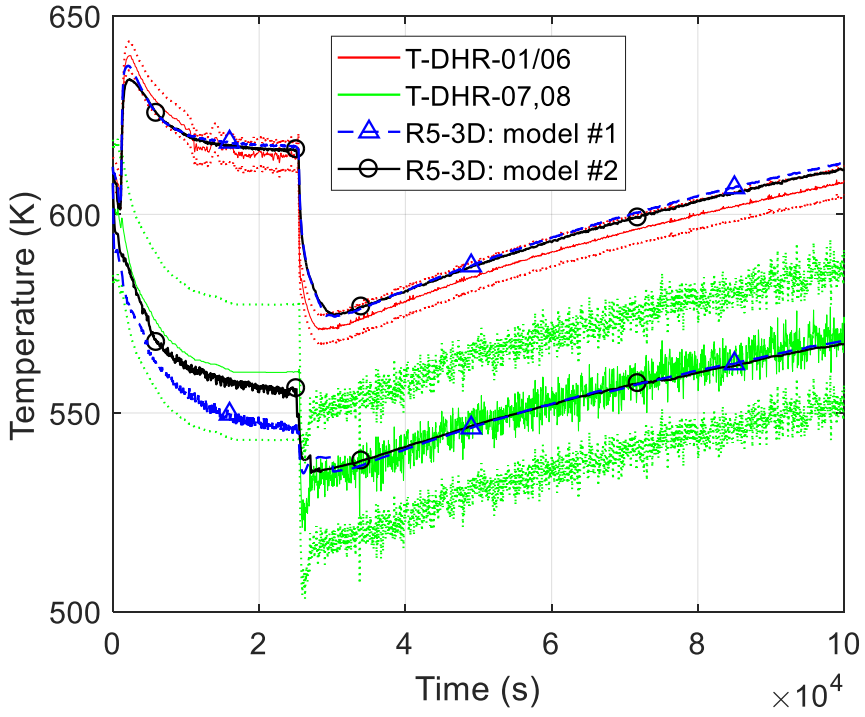

Fig. 20. TEST I: LBE DHR inlet/outlet temperature

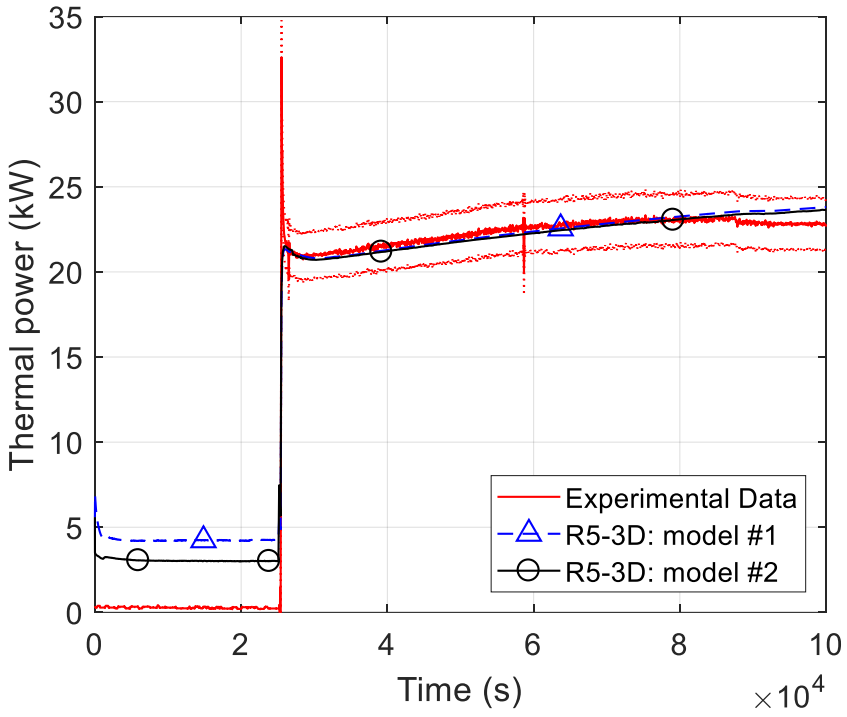

Fig. 21. TEST I: DHR power removed

In next figures the pool thermal stratification phenomenon is analyzed. Fig. 22 shows the full power steady state conditions obtained at 25000 s. The experimental trend is similar to the one observed in TEST A. Two relevant vertical stratifications occur along the HX shell (between 7 and 5 m) and at the HX outlet level (4 m from the pool bottom). The models provide results consistent with TEST A conclusions. Model #1 matches very well the temperature in the lower half part of the pool, where the discrepancies with experimental data are lower than 1 K. The middle stratification is obtained in the exact position (4 m) but the magnitude of the temperature plateau is under-predicted of about 15 K. In the upper part of the pool, model #1 provides a good estimation of the qualitative trend, but the difference with experimental temperature remains higher than 4 degrees up to the top. The MULTID component introduces improvements on the evaluation of the middle stratification. As shown in Fig. 26 (a), in the lower part of the pool the discrepancies with experimental data are lower than 1 degree. The calculated profile matches very well the measured temperatures up to 3.8 m, where the temperature plateau remains lower than experimental one of about 5 K. In the upper part, the multi-dimensional simulation matches the mono-dimensional one, under-predicting the experimental temperature of about 10 degrees up to the top of the pool (see also Fig. 26(a)).

After the transition, because of the loss of heat sink, LBE along the HX assumes quite uniform temperature that increases from 580 to 620 K along the transient test. The temperature inside the HX is comparable with the pool temperature and the decrease of heat losses leads to the attenuation of the upper thermal stratification. Fig. 23 shows the vertical temperature trend at 28000 s, after 3000 s from the transition event. The upper stratification disappears (uniform temperature of 573 K is observed between 3.5 and 7 m) and the middle stratification moves downward to the DHR outlet level. The transition is very well predicted by the two models. The mono-dimensional scheme obtains the maximum discrepancies at 3 m, where the LBE temperature is underestimated of about 4 K (within the error bands). In the upper part, a slight stratification effect is still observed between 6.5 and 7 m. The MULTID component provides a perfect agreement with experimental data. Fig. 25(b) shows a useful representation of the temperature inside the pool, highlighting the absence of the upper stratification and the movement of the middle one downstream the DHR outlet. In the upper part, a slight stratification is also observed between 6.5 and 7 m, where the maximum discrepancy with experiment occurs (see Fig. 26 (b)).

In NC operation the power removed by DHR plus the heat losses towards the environment are lower than FPS supplied power. The energy imbalance causes the temperature increase in the whole test facility, as shown in the previous figures. This evolution is also observed inside the pool, where the qualitative temperature profile is maintained over the whole transient, but the mean temperature increases. Fig. 24 shows the final conditions: the thermal stratification still occurs at 3.3 m from the bottom and the mean temperature increases to about 610 K. Both the models are able to reproduce the evolution inside the pool. At the end of the test a perfect agreement between the two calculations is observed. The stratification level is well defined in Fig. 25 (c) which shows the temperature representation in a relevant 2D section of the multi-dimensional component. The final conditions are well predicted by the code, limiting the discrepancies to a maximum value of 4 degrees (within the error bars), underestimated and overestimated respectively in the bottom and upper half part of the pool, as shown in Fig. 26 (c).

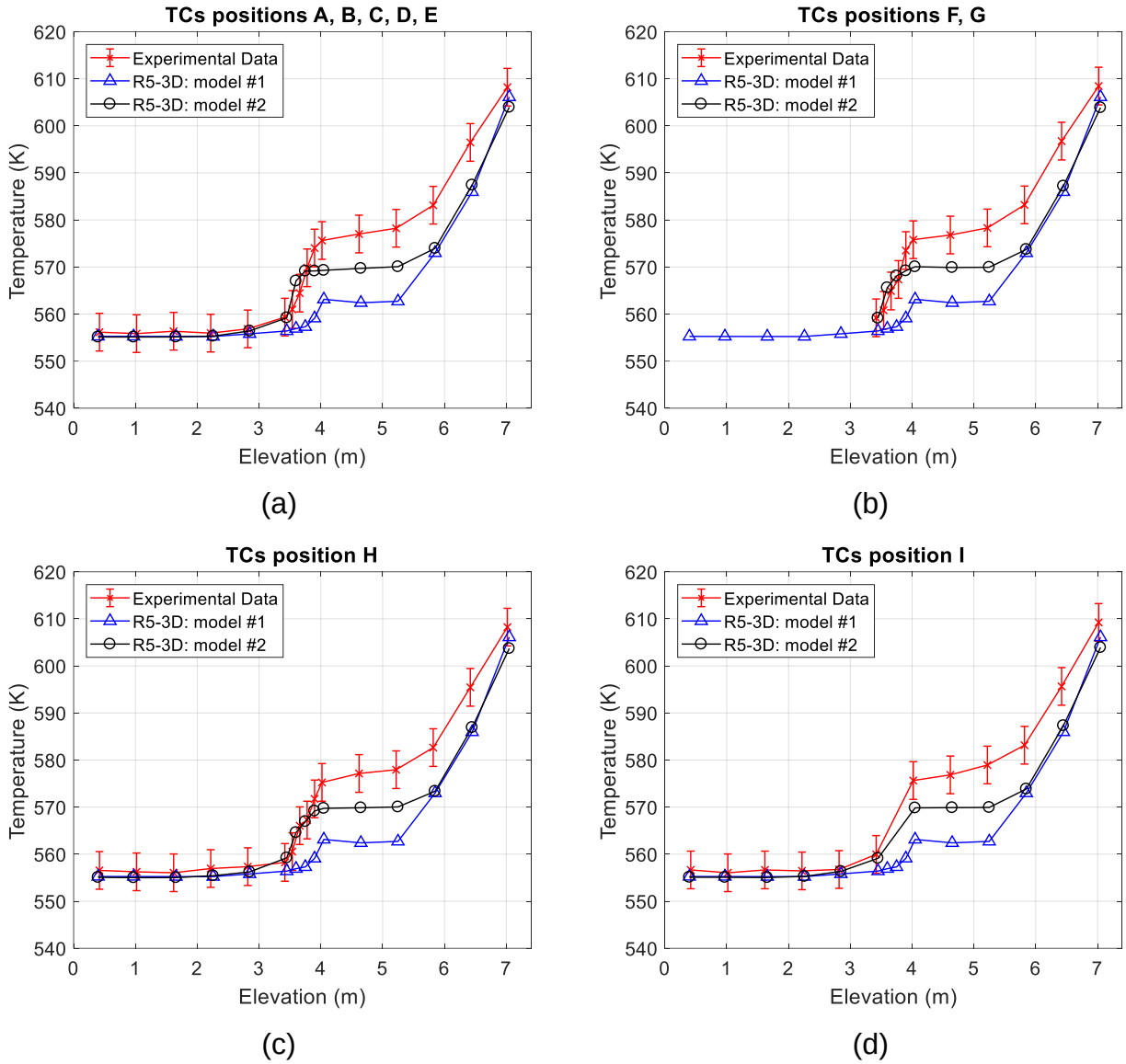

Fig. 22. TEST I: pool thermal stratification (25000 s)

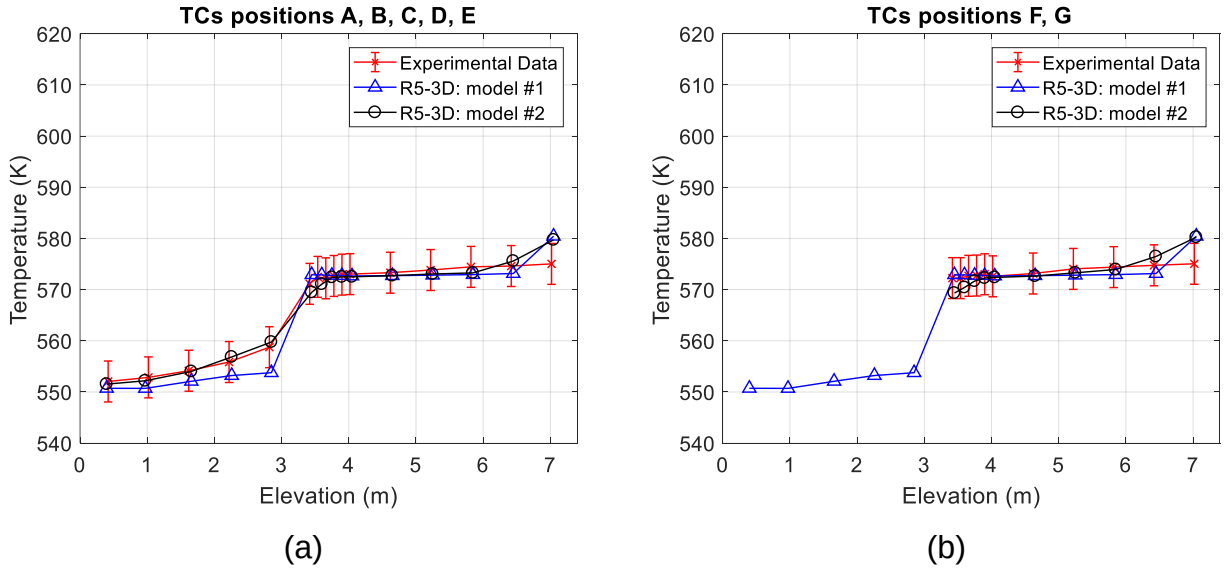

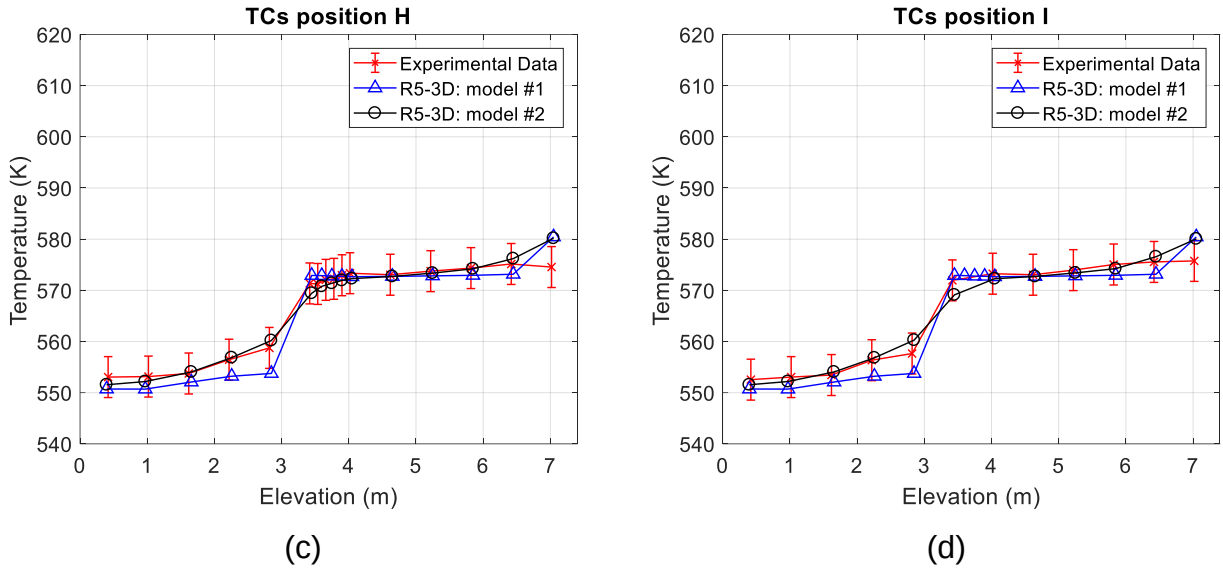

Fig. 23. TEST I: pool thermal stratification (28000 s)

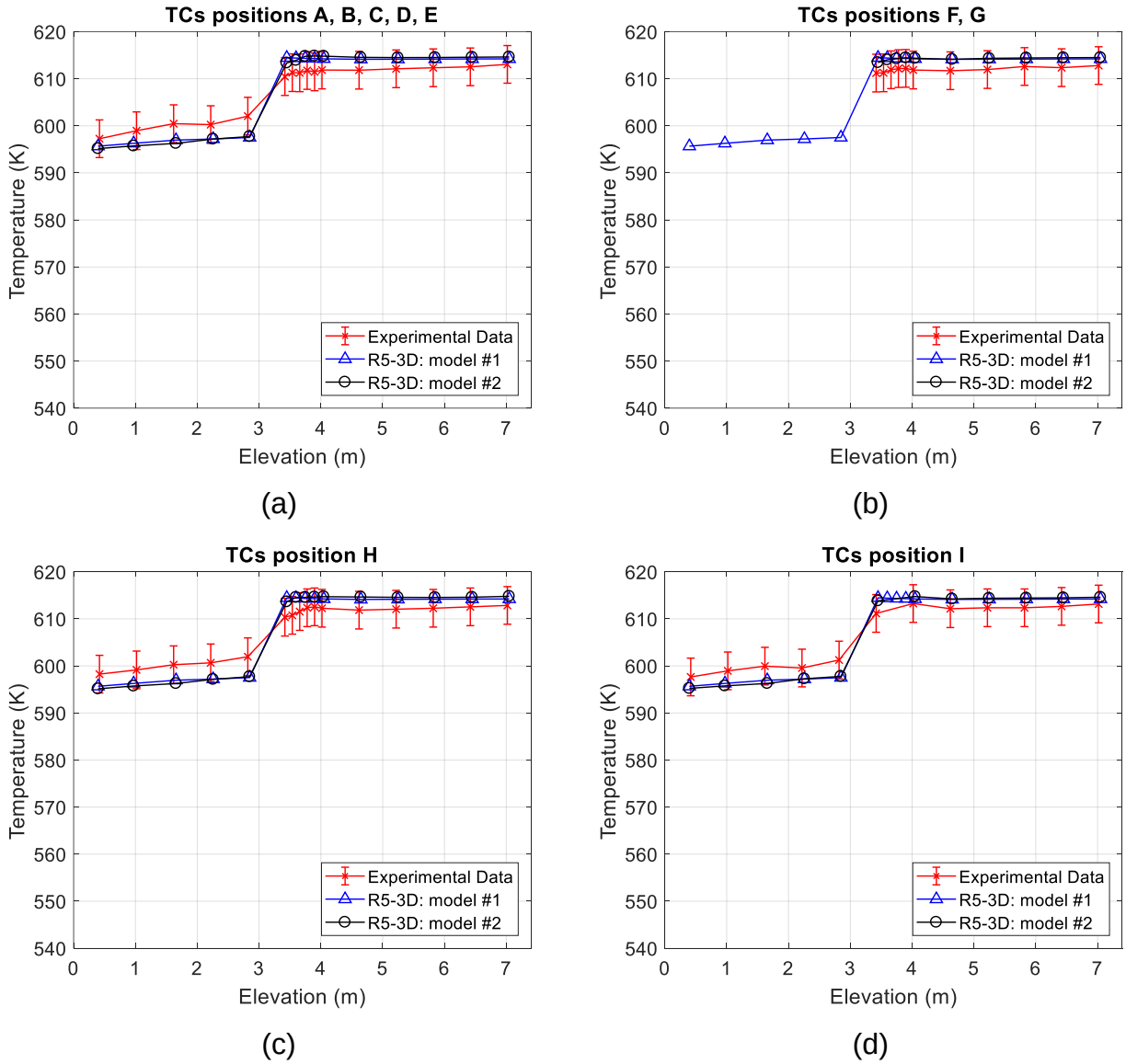

Fig. 24. TEST I: pool thermal stratification (100000 s)

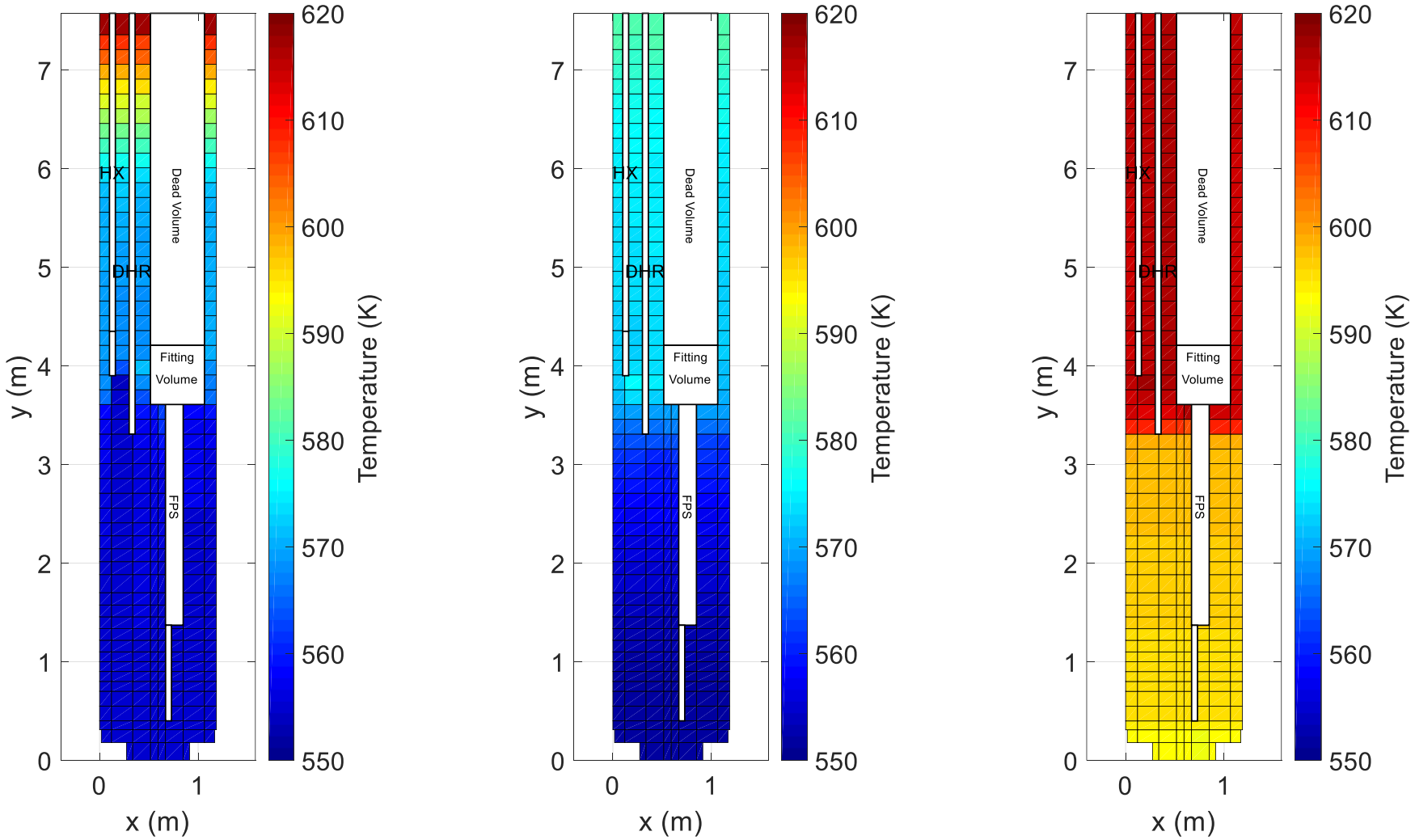

(a) 25000 s (b) 28000 s (c) 100000 s

Fig. 25. TEST I: pool temperature, model #2

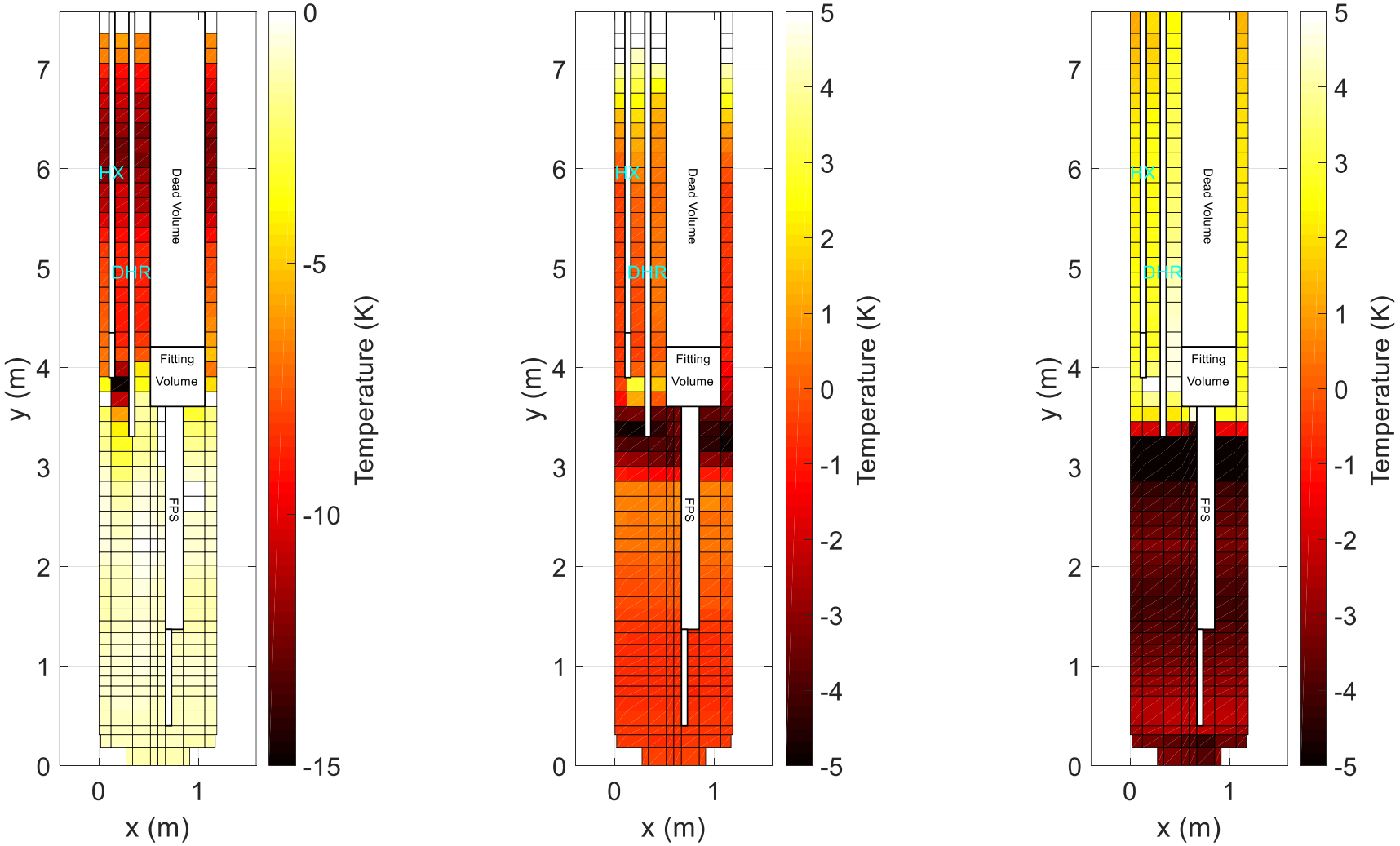

(a) 25000 s

(b) 28000 s

(c) 100000 s

Fig. 26. TEST I: error distribution map, model #2

5. Modelling analysis

5.1 Time step and mesh sensitivities

Fig. 27 shows the time step sensitivity performed with model #1; time step has been set to 0.005, 0.002 and 0.001 s. Six relevant parameters have been considered to verify time step effect on the accuracy of the simulations: LBE mass flow rate (Fig. 27(a)), FPS inlet and outlet temperature (Fig. 27(b)), HX inlet and outlet temperature (Fig. 27(c)) and thermal stratification profile within the pool. The calculations reproduce the full power operation of TEST I and the comparison with experimental data is shown. The three calculations highlight a perfect matching, proving that the accuracy of the results is not affected by the time step.

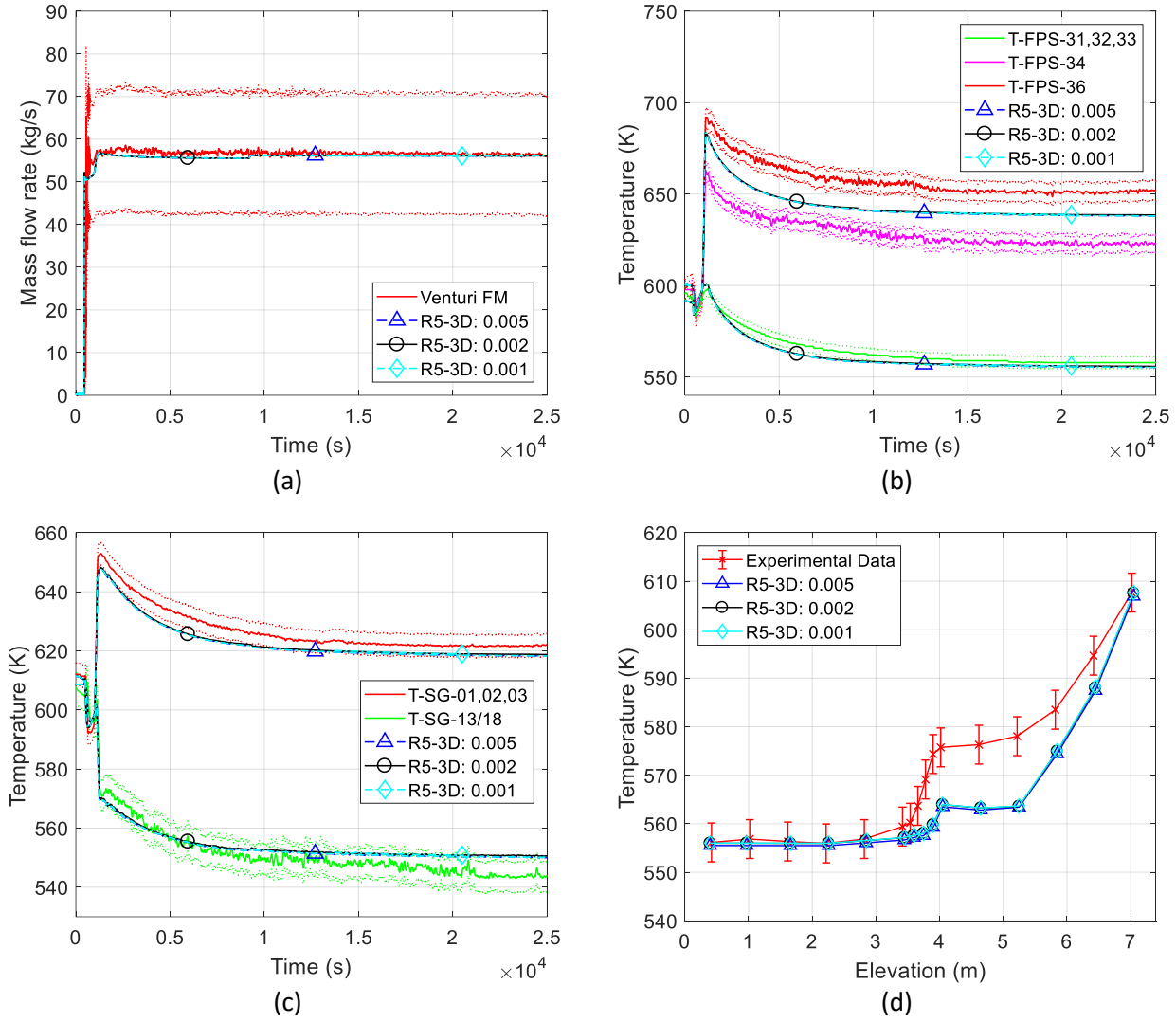

Fig. 27. Time step sensitivity

The same figures of merit have been considered to assess the effect of the mesh discretization on the accuracy of the results. The mesh sensitivity concerns the FPS, riser and HX modelling, as described in section 3. Fig. 28 shows the comparison of the calculations with experimental data. In the plots, the mesh resolution is specified in the legend. The study highlights negligible effect of the mesh on the accuracy of the calculations.

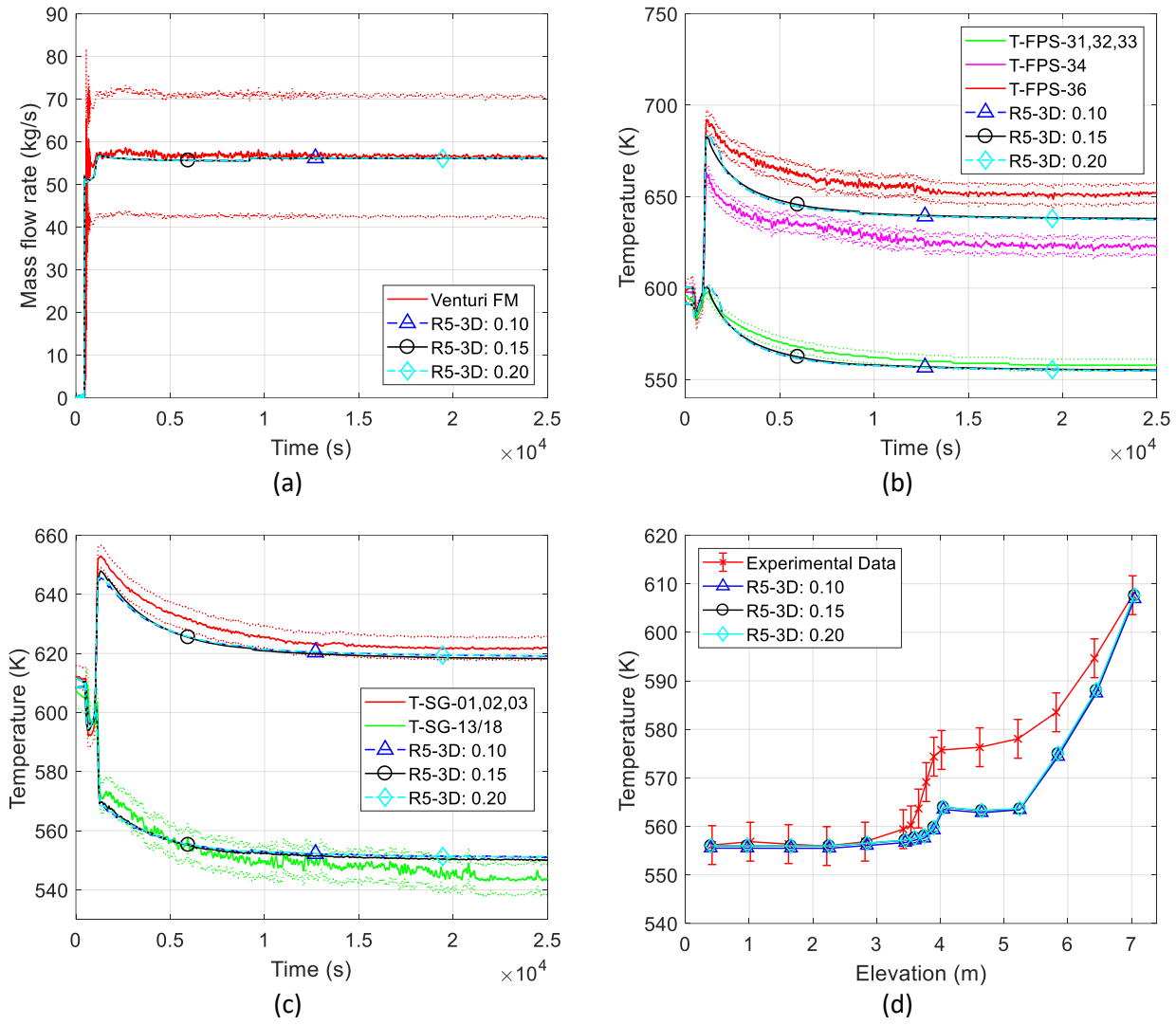

Fig. 28. Mesh sensitivity

5.2 FPS radial conduction

In model #2 the FPS subchannel modelling has been introduced. As presented in section 3, calibrated heat structures have been implemented to consider radial conduction that could play a crucial role on the evaluation of temperature distribution through the FPS.

The capabilities of RELAP5 as subchannel analysis code were assessed by Memmott (2010). In this work, the influence of heat conduction on axial and radial directions was investigated. Calculations showed that axial conduction had not effects on the temperature distribution through the fuel bundle and radial heat conduction presented negligible effects assuming high mass flow rate but significant improvement for low coolant mass flow rate. Peclet number represents the ratio between the magnitude of heat convection and radial heat conduction; radial conduction assumes relevant effect when Pe < 1. For the evaluation of the axial conduction influence, Yoo (2013) proposed a modified expression of Peclet number ($Pe^* = Re\ Pr\ L/D_h$); axial conduction must be accounted when Pe^* < 100.

In CIRCE-ICE experiment, Pe and Pe^* assume values equal to 2005 and 106940 in GEC operation and 300 and 16043 in NC condition. Pe^* is significantly higher than 100 in both GEC and NC operations and the axial contribution has not been considered in the analysis.

Radial heat conduction also should not have relevant effects on the calculations; this aspect has been assessed.

Fig. 29(a) shows the temperature distribution calculated by R5-3D with radial conduction at the end of the HS active length, in GEC operation. As expected, due to the uniform supply of the thermal power, a flat temperature distribution is obtained in the inner zone of the bundle but a sharp temperature decrease (30 K) is observed approaching the hexagonal shell. Fig. 29(b) depicts the temperature difference between the case with radial conduction and the case without heat conduction. At full power operation, when the LBE mass flow rate is 56 kg/s, discrepancies between the calculations are negligible, limiting the maximum difference to 1.2 K (in the corner and edge subchannels). Fig. 30 compares the temperature profile in the radial direction obtained by the two calculations. In the same plot, temperature measured by TCs and the error bars, representing the uncertainties on the temperature acquisitions and the instrument positions are reported. A good agreement with experimental data is observed with both the calculations. Radial conduction tends to smooth the temperature profile, but this effect is practically negligible.

The same analysis is carried out in NC operation, when the LBE mass flow rate is about 7 kg/s. Due to the low value of power, the temperature difference between the inner and edge subchannels is reduced to about 5 degrees (see Fig. 31(a) representing the calculation assuming radial conduction). In this case, the effect of the radial conduction is slightly higher than the GEC condition. Fig. 31(b) shows that maximum discrepancy between two calculations increases to about 2.5 K in the edge subchannels. In Fig. 32 the effect of the thermal conductivity is visible, flattening the temperature profile at the HS exit. Some discrepancies are observed with the experimental data, but the radial heat conduction provides a better estimation of the qualitative profile and it reduces the discrepancies on the bundle edge.

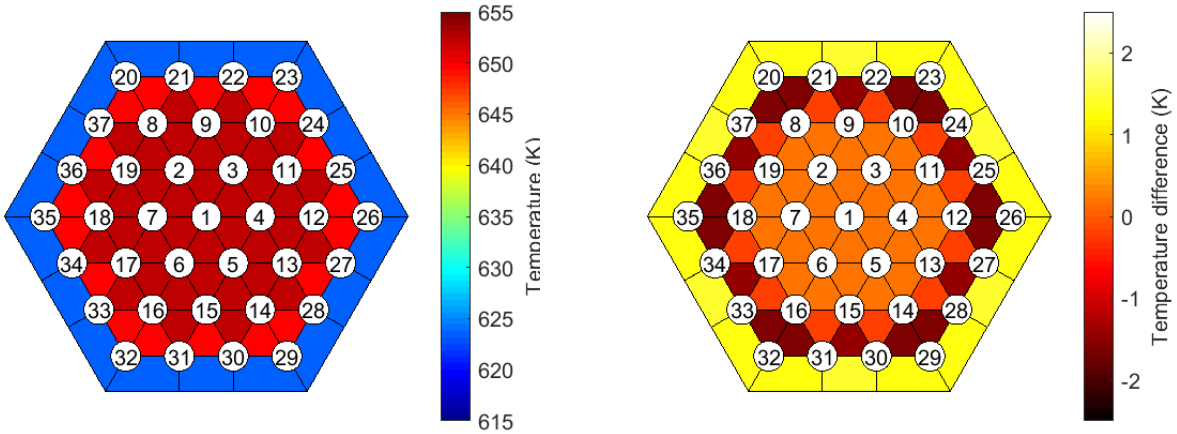

(a) (b)

Fig. 29. FPS outlet temperature: radial conduction effect (20000 s)

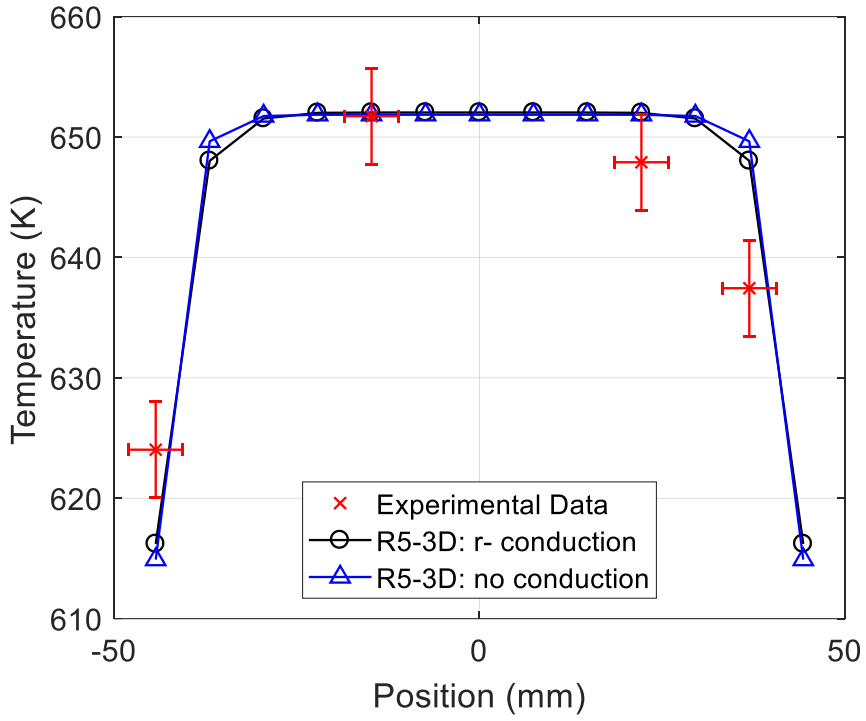

Fig. 30. FPS outlet temperature: comparison with experimental measurements (20000 s)

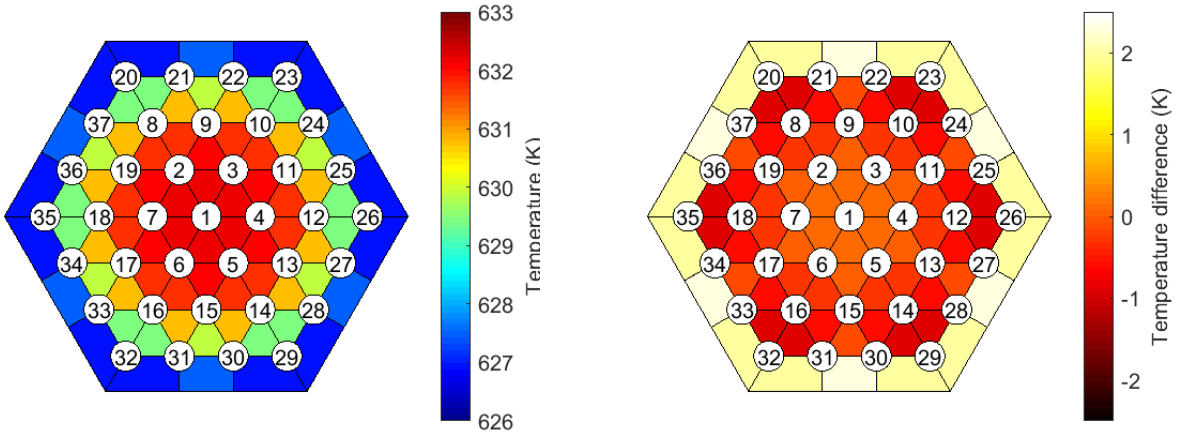

(a) (b)

Fig. 31. FPS outlet temperature: radial conduction effect (89000 s)

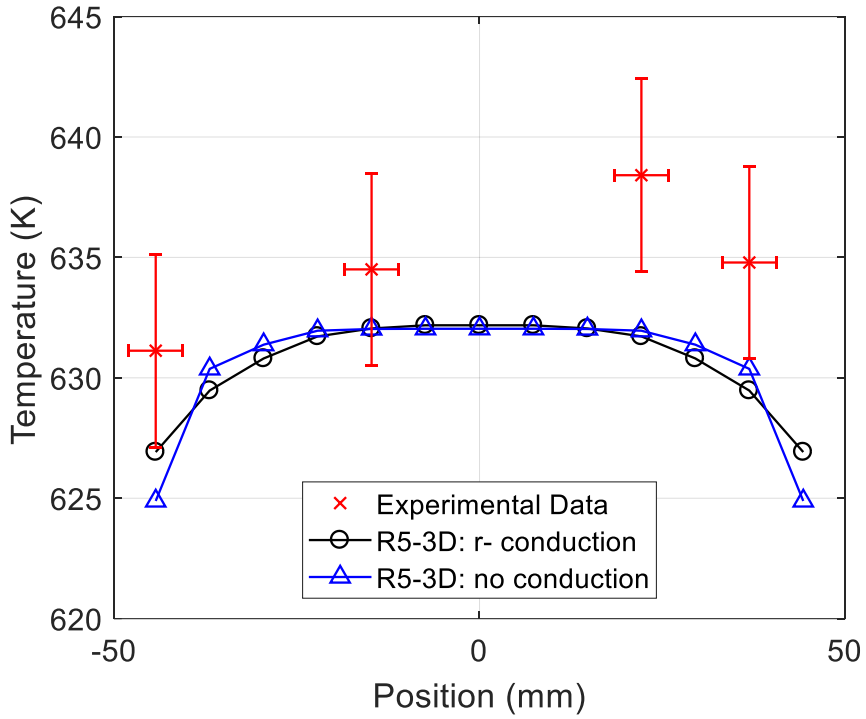

Fig. 32. FPS outlet temperature: comparison with experimental measurements (89000 s)

5.3 Pool modelling

RELAP5-3D capabilities on the prediction of relevant phenomena into large pool have been investigated, evaluating the best practice for the pool simulation. The simplest approach is to reproduce LBE pool with a single vertical pipe. As mentioned in section 1, a thermal stratification model was introduced in RELAP5-3D to improve the solutions when a separation of hot and cold liquid layers appears in a vertical stack of cells (The RELAP5-3D© Code Development Team, 2015a). In Fig. 33 this option is investigated, comparing two calculations: disabled model (R5-3D in Fig. 33) and thermal stratification model (R5-3D: t). In addition, due to the quasi-stagnant conditions within the pool, thermal conduction could play a crucial role. For this purpose, the effect of the vertical conduction is assessed introducing heat structures between each pool cell, assuming a dummy material with negligible heat capacity and LBE thermal conductivity, the LBE volume of the nodalization and a high HT multiplicative factor to reduce the convective resistance. Fig. 33 shows good prediction in the lower part (between 0 and 2.5 m), where the difference with experimental data are limited to 1 degree, and in the upper part (between 5.5 and 7 m), where the error is higher (about 6 K) but the qualitative trend is well reproduced. Relevant discrepancies are observed in the middle zone. In this region, the large amount of the heat losses from the hot leg causes a prompt temperature increase at 3.8 m. A single pipe is not able to simulate buoyancy and mixing convection, resulting in a stagnant LBE inside the pool, where the upward flow of the hot liquid is not allowed. The activation of thermal stratification model does not produce improvement on the accuracy of the simulations while the implementation of the vertical conduction reduces the thermal peak at 3.8 m but large discrepancy with experiment is still observed.

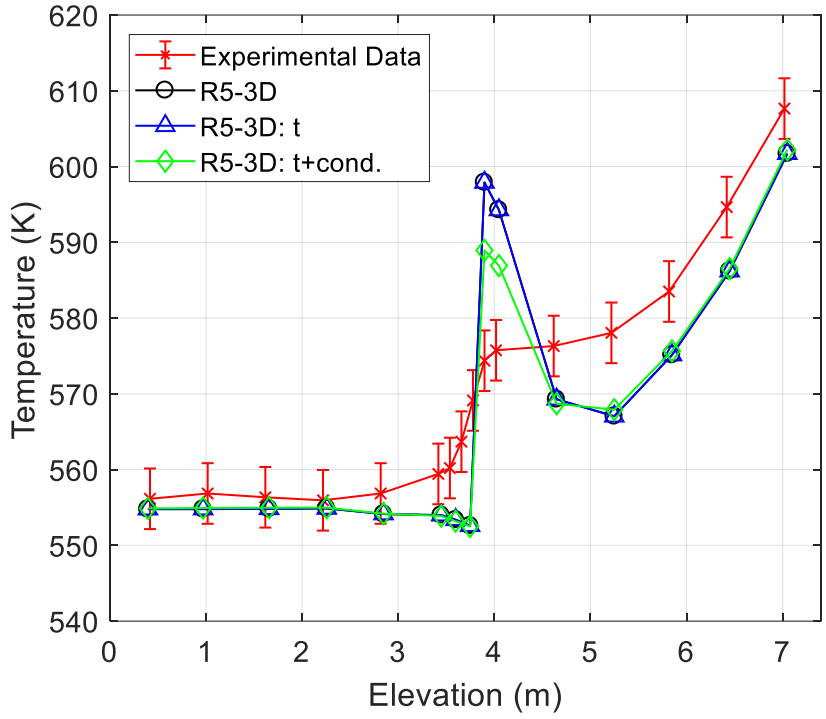

Fig. 33. Pool modelling: single pipe

Examples of RELAP5 applications on the thermal stratification simulation in large tanks were found in literature, highlighting capabilities of the code to reproduce this phenomenon with multiple channels and several cross junctions. This approach has been applied in CIRCE-ICE modelling, considering two different nodalization scheme. Model #1.0 consists of 3 parallel pipes and 156 cross junctions. The axial discretization is the same presented in section 3 but, in this case, one vertical channel includes the central part of the pool, in contact with the whole test section, an the other two simulate the pool edge, thermally connected with the external environment. The second modelling approach, model #1, has been presented in section 3. The results of the simulations are presented in Fig. 34. In addition, the vertical conduction model is implemented in model #1 to assess the magnitude of this effect (radial conduction has not been considered because it is expected to be not relevant due to the temperature distribution uniformity at the same axial level). Fig. 34 shows good agreement between the calculations in the lower and upper part of the pool. In the middle zone, model #1.0 does not predict the temperature plateau because the cold LBE exiting the HX is mixed with the LBE inside the pool, decreasing the temperature and causing the low peak at 3.8 m. On the model #1, thermal conduction does not affect the computational results because mixing phenomena induce to larger order of magnitude thermal effects. On the other hand, the implementation of the conduction model increases the model run time of 7.5%.

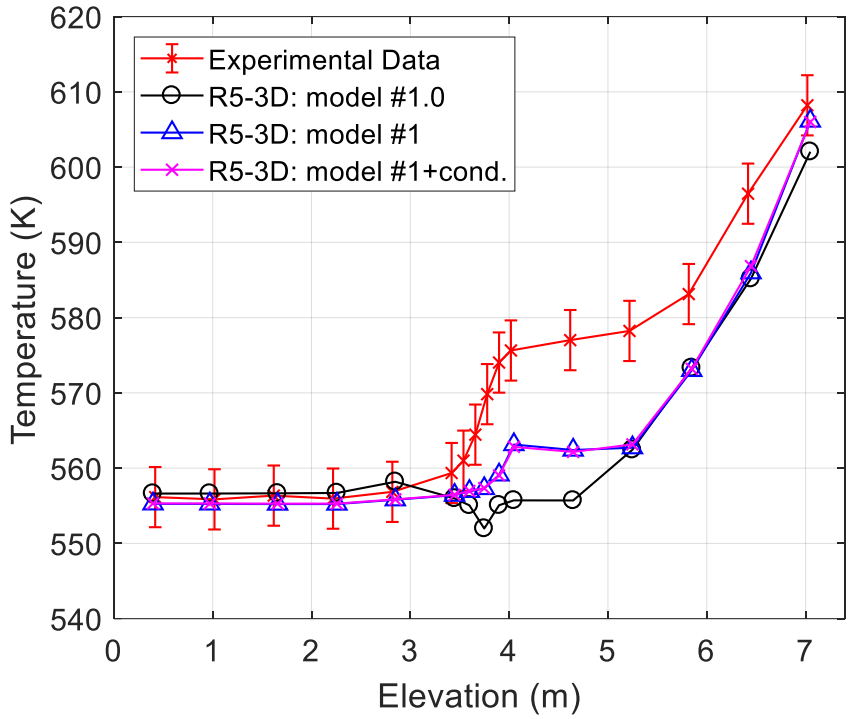

Fig. 34. Pool modelling: three parallel pipes with cross junctions

In model #2 a multi-dimensional component has been introduced to reproduce CIRCE pool. RELAP-3D allows to use two sets of momentum equations within MULTID component: three-dimensional momentum equations or mono-dimensional momentum equations (in this case they are applied on each of the coordinate directions) (The RELAP5-3D© Code Development Team, 2015b). In Fig. 35 the influence of the momentum equations set is assessed. The discrepancies between the calculations are limited in the middle zone of the pool and the magnitude of the differences is about 1 degree. In particular, the use of 1D momentum equations (R5-3D: 1D in Fig. 35) led to an under-prediction of the temperature plateau during the GEC operation (see Fig. 35(a)). After the transition, two simulations highlight good agreement; low differences are observed between 0 and 3 m from the bottom of the pool (Fig. 35(b)).

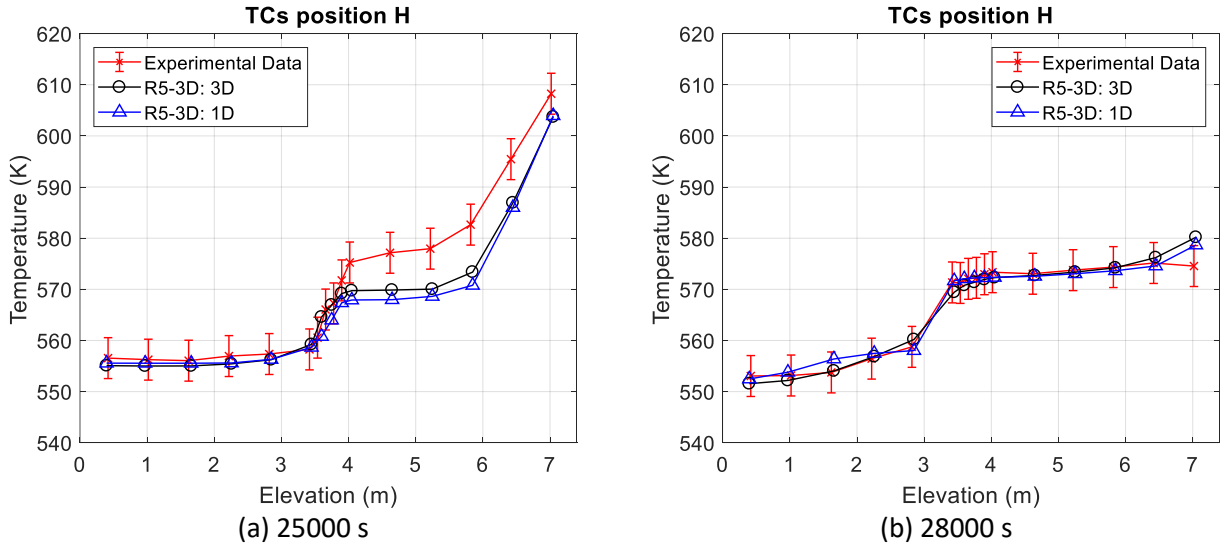

Fig. 35. Influence of the momentum equations

6. Conclusions

The experimental campaign promoted in CIRCE-ICE test facility was aimed to investigate the thermal-hydraulics of a complex HLM system and to provide data for validation of computational tools. Two experimental tests have been analyzed in this paper: TEST A consisting in a transition from no-power to full power steady state conditions, and TEST I, consisting in a transition from GEC to NC, simulating a protected loss of heat sink plus a loss of flow accident. The aim of the computational activity has been to investigate the capability of RELAP5-3D© to predict thermal stratification phenomenon in an HLM pool.

Several examples were found in literature concerning the simulation of large tanks with RELAP5. A thermal stratification model was implemented in RELAP5 that, allows an accurate evaluation of the phenomenon in a tank. The two models can be only applied to vertically oriented components without cross junctions. Even if this approach provided good results on the simulation of tanks with limited volume, such as a pressurizer, it highlighted some limits on the simulation of large pools. In this case, a better evaluation of the thermal stratification was found simulating the pool with multiple vertical channels with cross junctions, not allowing the application of thermal stratification model. In this paper, the two modelling methods are applied and compared with an additional approach consisting in the application of the multi-dimensional component for the simulation of the pool.

The state of art on the simulation of the thermal stratification in large pool has been confirmed by the calculation performed on CIRCE-ICE. The mono-dimensional approach, using a single channel for the pool modelling, highlights discrepancies with the experimental data, failing on the prediction of the axial temperature profile. A high peak temperature in the middle of the tank which is not observed by the experiment is caused by a total absence of the natural flow within the pool. In order to verify how the axial conduction within the fluid can improve the computational results, a thermal conduction model has been implemented in the nodalization, using several heat structures that couple adjacent meshes. As expected, the axial conduction reduces the peak but not enough to match the experimental temperature profile.

In order to allow natural circulation inside the pool, the second approach has been applied, dividing the pool in three vertical channels connected with cross junctions. Two nodalization schemes have been presented for the discretization of the pool. This approach has shown good capabilities on the thermal stratification evaluation. The qualitative trend is well reproduced, predicting two relevant stratification in the upper and in the middle volumes of

the pool. In the lower part of the tank, the LBE temperature is very well simulated but, at 4 m, the plateau temperature is underpredicted of about 15 K and this discrepancy is maintained up to the cover gas.

RELAP5-3D capabilities were improved with a fully integrated multi-dimensional modelling scheme, mainly developed for volumes where the movement of the fluid is preferably 1D. In this activity the MULTID component has been used for the simulation of CIRCE pool. The nodalization scheme is the same of model #1 except for the pool, simulated with a detailed three-dimensional component, and the FPS, where subchannel division has been performed.

The same boundary conditions have been applied to model #1 and #2, reproducing the two experimental transient tests. Several figures of merit have been selected, assessing the capabilities of the two models to reproduce thermal-hydraulics of an HLM cooled pool-type system in safety relevant operations. The comparison with experimental data has highlighted excellent capabilities of the two models to predict the thermal-hydraulics of the main flow path, managing to evaluate the most important features: LBE mass flow rate in both GEC and NC conditions, heat exchange within FPS, HX and DHR, and heat losses. In each condition, the computational results are included within the experimental error band. In addition, model #2 assesses RELAP5-3D abilities as a subchannel analysis code, in both GEC and NC operations. The effect of the radial conduction has been evaluated implemented a thermal conduction model, using heat structures. This analysis has shown small effects of the radial conduction, even if, in low flow rate regimes, such as NC operation, it provides not negligible improvement on the prediction of the temperature profile. In this case the simulation is in good agreement with experimental data; the highest discrepancies are observed in the edge of the bundle (4 degrees) where the errors can be justified by the uncertainties related to the TCs positions.

Focusing on the pool simulation, the MULTID component has introduced relevant improvements on the prediction of the thermal stratification phenomenon. The two relevant stratifications have been observed by the calculation. The temperature in the lower part matches very well the experimental measurements. The lower stratification level is well predicted and the temperature hot plateau underestimation has been reduced to 5 K. After the transition from GEC to NC, both the models are able to predict the upper stratification attenuation and the movement of the lower one below the DHR outlet. In the long term, the two calculations provide the same temperature profile that matches well the experimental

trend, limiting the discrepancies below 4 degrees. Evaluation of the axial conduction within the pool has been performed, highlighting limited effects, especially when the natural circulation inside the pool is considered.

In conclusion, RELAP5-3D shows good capabilities on the prediction of the thermal stratification by modelling the pool with multiple channels with cross junctions or with a multi-dimensional component. The natural circulation within the pool seems to play a crucial role for the thermal stratification instauration. The qualitative temperature profile is well reproduced by the two approaches but the multi-dimensional nodalization reduces discrepancies with the experimental data. The discrepancies seem due to a not perfect evaluation of the heat losses through the wall of the internal component. In this frame, the implementation of a specific correlation for the heat transfer coefficient evaluation in large volumes could play a crucial role on the accuracy of the results.

Acknowledgements

The authors wish to thank all the ENEA FSN-ING and in particular M. Tarantino for providing CIRCE-ICE experimental data. The work was partially funded by the Italian Programme Agreement on Electric System Research between ENEA and the Italian Ministry for Economic Development.

References

Agostini, P., Alemberti, A., Ambrosini, W., Benamati, G., Bertacci, G., Cinotti, L., Elmi, N., Forgione, N., Oriolo, F., Scadozzo, G., Tarantino, M., 2005. Testing and qualification of CIRCE Venturi-nozzle flow meter for large scale experiments. Proc. 13th Int. Conf. Nucl. Eng., Beijing, China. DOI: 10.1115/ICONE13-50909

Ahn, J.S., Bluck, M., Eaton M., Jackson, C., 2018. A validation of RELAP on predicting nuclear power plant phenomena. Proc. 26th Int. Conf. Nucl. Eng., London, England. DOI: 10.1115/ICONE26-81424

Ambrosini, W., Azzati, M., Benamati, G., Bertacci, G., Cinotti, L., Forgione, N., Oriolo, F., Scadozzo, G., Tarantino, M., 2004. Testing and qualification of CIRCE instrumentation based on bubble tubes. Jou. Nuc. Mat. 335, 293-298. doi:10.1016/j.jnucmat.2004.07.030

Angelucci, M., Martelli, D., Barone, G., Di Piazza, I., Forgione, N., 2017. STH-CFD Codes Coupled Calculations Applied to HLM Loop and Pool Systems. Sci. Tech. Nucl. Ins., Vol. 2017, doi: 10.1155/2017/1936894

Baik, S.J., Lee, K.W., Ro, T.S. Thermal stratification in the pressurizer. Retrieved from https://inis.iaea.org/collection/NCLCollectionStore/_Public/32/068/32068795.pdf

Bayless, P.D., et al., 2015. RELAP5-3D Code Manual Vol. III: Developmental Assessment. INL/MIS-15-36723 Volume I, Revision 4.3

Balestra, P., Giannetti, F., Caruso, G., Alfonsi, A., 2016. New RELAP5-3D lead and LBE thermophysical properties implementation for safety analysis of Gen IV reactors. Sci. Technol. Nucl. Install. 2016. DOI: 10.1155/2016/1687946

Bandini, G., Polidori, M., Meloni, P., Tarantino, M., Di Piazza, I., 2015. RELAP5 and SIMMER-III code assessment on CIRCE decay heat removal experiments. Nucl. Eng. Des. 281, 39-50. http://dx.doi.org/10.10167j.nucengdes.2014.11.005

D'Auria, F., 2017. Thermal-hydraulics of water cooled nuclear reactors (First edit). Duxford; Cambridge, MA: Woodhead Publishing. Retrieved from https://www.sciencedirect.com/book/9780081006627/thermal-hydraulics-of-water-cooled-nuclear-reactors#book-description

Edemetti F., Tassone, A., Narcisi, V., Giannetti, F., Ferroni, L., Tarantino, M., 2018. Numerical analysis of temperature stratification in the CIRCE pool facility. Proc. 36th UIT Heat Trans. Conf.

Frogheri, M., Alemberti, A., Mansani, L., 2013. The advanced lead fast reactor European demonstrator (ALFRED). Proc. 15th Int. Top. Meet. Nucl. React. Therm. - Hydraul. Int. Top. Meet. Nucl. React. Therm. - Hydraul. Pisa, Italy

Giannetti, F., Di Maio, D.V., Naviglio, A., Caruso, G., 2016. Thermal-hydraulic analysis of an innovative decay heat removal system for lead-cooled fast reactors. Nucl. Eng. Des. 305, 168-178. http://dx.doi.org/10.1016/j.nucengdes.2016.05.005

Harten, A., 1989. ENO schemes with subcell resolution. Jour. Comp. Phy. 83, 148-184. https://doi.org/10.1016/0021-9991(89)90226-X

Kadambi, C.E.R.S.N.H.S.S.L.N.P., 1988. Bulletin 88-11: pressurizer surge line thermal stratification. Retrieved from https://www.nrc.gov/reading-rm/doc-collections/gen-comm/bulletins/1988/bl88011.html

Kazimi, M.S., Carelli, M.D., 1976. Clinch River Breeder Reactor Plant Heat Transfer Correlation for Analysis of CRBRP Assemblies, CRBRP-ARD-0034, Westinghouse.

Kim, S.N., 1984. An experimental and analytical model of a PWR pressurizer during transients. Massachusetts Institute of Technology. Retrieved from https://dspace.mit.edu/handle/1721.1/15611

Kumar, S., Vijayan, P.K., Kannan, U., Sharma, M., Pilkhwal, D.S., 2017. Experimental and computational simulation of thermal stratification in large pools with immersed condencer. App. Therm. Eng. 113, 345-361. http://dx.doi.org/10.1016/j.applthermaleng.2016.10.175

Idelchik, I.E., 1986. Handbook of Hydraulic Resistance. Second ed. Hemisphere Publishing Corporation.

Martelli, D., Forgione, N., Di Piazza, I., Tarantino, M., 2015. HLM fuel pin bundle experiments in the CIRCE pool facility. Nucl. Eng. Des. 292, 76-86. http://dx.doi.org/10.1016/j.nucengdes.2015.06.004

Martelli, D., Tarantino, M., Di Piazza, I., 2016. Experimental activity for the investigation of mixing and thermal stratification phenomena in the CIRCE pool facility. Proc. 24th Int. Conf. Nucl. Eng., Charlotte, North Carolina, USA. DOI: 10.1115/ICONE24-60920

Memmott, M., Buongiorno, J., Hejzlar, P., 2010. On the use of RELAP5-3D as a subchannel analysis code. Nucl. Eng. Des. 240, 807-815. Doi:10.1016/j.nucengdes.2009.11.006

Narcisi, V., Giannetti, F., Tarantino, M., Martelli, D., Caruso, G., 2017. Pool temperature stratification analysis in CIRCE-ICE facility with RELAP5-3D© model and comparison with experimental tests. J. Phys. Conf. Ser. 923 (012006). DOI: 10.1088/1742-6596/923/1/012006

Narcisi, V., Giannetti, F., Del Nevo, A., Tarantino, M., Caruso, G., 2018. Pre-test analysis of accidental transients for ALFRED SGBT mock-up characterization. Nucl. Eng. Des. 333, 181-195. DOI: 10.1016/j.nucengdes.2018.04.015

OECD/NEA Nuclear Science Committee, 2015. Handbook on Lead-bismuth Eutectic Alloy and Lead Properties, Materials Compatibility, Thermal-hydraulics and Technologies. https://www.oecd-nea.org/science/pubs/2015/7268-leadbismuth-2015.pdf

OECD Nuclear Energy Agency – GIF, 2017. GIF Annual Report 2017. https://www.gen-4.org/gif/upload/docs/application/pdf/2018-09/gif_annual_report_2017_210918.pdf.

Press W.H., Teukolsky S.A., 1990. Savitzky-Golay Smoothing Filters. Comp. Phy. 4, 669-672. doi: 10.1063/1.4822961

Saedi, H.R., 1983. Insurge pressure response and heat transfer for PWR pressurizer. Massachusetts Institute of Technology. Retrieved from https://dspace.mit.edu/handle/1721.1/15523

Schikorr, M., Bubelis, E., Mansani, L., Litfin, K., 2010. Proposal for pressure drop prediction for a fuel bundle with grid spacers using Rehme pressure drop correlations. Nucl. Eng. Des. 240, 1830-1842, DOI: 10.1016/j.nucengdes.2010.03.039, 2010

Schuler, X., Herter, K.H., 2004. Thermal fatigue due to stratification and thermal shock loading of piping. In 30th MPA-Seminar in conjunction with the 9th German-Japanese Seminar. Retrieved from https://inis.iaea.org/collection/NCLCollectionStore/_Public/36/036/36036665.pdf

Shumway, R., Bolander, M., Aktas B., 2002. Prediction of MIT Pressurizer Data using RELAP5 and TRAC-M. Proc. 10th Int. Conf. Nucl. Eng., Arlington, VA, USA. doi:10.1115/ICONE10-22580

Tarantino, M., Martelli, D., Barone, G., Di Piazza, I., Forgione, N., 2015. Mixed convection and stratification phenomena in a heavy liquid metal pool. Nucl. Eng. Des. 286, 261-277. DOI: 10.1016/j.nucengdes.2015.02.012

Tarantino, M., Agostini, P., Benamati, G., Coccoluto, G., Gaggini, P., Labanti, V., Venturi, G., Class, A., Liftin, K., Forgione, N., Moreau, V., 2011. Integral Circulation Experiment: Thermal-hydraulic simulator of a heavy liquid metal reactor. Jou. Nucl. Mat. 415, 433-448. DOI: 10.1016/j.jnucmat.2011.04.033

The RELAP5-3D© Code Development Team, 2015a. RELAP5-3D Code Manual Vol. I: Code Structure, System Models, and Solution Methods. INL/MIS-15-36723 Volume I, Revision 4.3

The RELAP5-3D© Code Development Team, 2015b. RELAP5-3D Code Manual Vol. IV: Models and correlations. INL/MIS-15-36723 Volume IV, Revision 4.3

Thuy, N.T.T., Trung, T.V., Dien, L.D., 2012. Investigation of temperature stratification in cold leg and downcomer in LSTF/ROSA experiment. Retrieved from https://inis.iaea.org/collection/NCLCollectionStore/_Public/45/058/45058897.pdf

Turroni, P., Cinotti, L., Corsini, G., Mansani, L., 2001. The CIRCE test Facility, in: ANS Winter Meeting AccApp. Reno, Nevada, USA

Ushakov, P.A, Zhukov, A.V., Matyukhin, N.M., 1977. Heat transfer to liquid metals in regular arrays of fuel elements. High Temp. 15, 868-873 translated from Teplofizika Vysokikh Temperatur 15 (1977), 1027-1033

Verma, P.K., Nayak, A.K., Jain, V., Vijayan, P.K., Vaze, K.K., 2013. Suppression of thermal stratification in gravity driven water pool of an advanced reactor using shrouds. Ann. Nucl. En. 58, 221-227. http://dx.doi.org/10.1016/j.anucene.2013.03.012

Yoo Y.J., Sabharwall P., Reyes J.N., Wu Q., Sienicki J.J., 2003. Effects of the fluid axial conduction on liquid metal natural circulation and linear stability. In: 2003 ANS/ENS International Winter Meeting, New Orleans, LA, pp. 1523-1530.